Dynamics and fragmentation of van der Waals and hydrogen bonded cluster cations: $(NH_3)_n$ and $(NH_3BH_3)_n$ ionized at 10.51 eV

Bing Yuan, Joong-Won Shin, and Elliot R. Bernstein'

Citation: The Journal of Chemical Physics **144**, 144315 (2016); doi: 10.1063/1.4945624
View online: http://dx.doi.org/10.1063/1.4945624
View Table of Contents: http://aip.scitation.org/toc/jcp/144/14
Published by the American Institute of Physics

Dynamics and fragmentation of van der Waals and hydrogen bonded cluster cations: $(NH_3)_n$ and $(NH_3BH_3)_n$ ionized at 10.51 eV

Bing Yuan,[1] Joong-Won Shin,[2] and Elliot R. Bernstein[1,a)]
[1]*Department of Chemistry, Colorado State University, Fort Collins, Colorado 80523-1872, USA*
[2]*Division of Chemistry and Biological Sciences, Governors State University, University Park, Illinois 60484-0975, USA*

(Received 4 January 2016; accepted 25 March 2016; published online 14 April 2016)

A 118 nm laser is employed as a high energy, single photon (10.51 eV/photon) source for study of the dynamics and fragmentation of the ammonia borane (NH_3BH_3) cation and its cluster ions through time of flight mass spectrometry. The behavior of ammonia ion and its cluster ions is also investigated under identical conditions in order to explicate the ammonia borane results. Charge distributions, molecular orbitals, and spin densities for $(NH_3BH_3)_n$ and its cations are explored at both the second-order perturbation theory (MP2) and complete active space self-consistent field (CASSCF) theory levels. Initial dissociation mechanisms and potential energy surfaces for ionized NH_3BH_3, NH_3, and their clusters are calculated at the MP2/6-311++G(d,p) level. Protonated clusters $(NH_3)_xH^+$ dominate ammonia cluster mass spectra: our calculations show that formation of $(NH_3)_{n-1}H^+$ and NH_2 from the nascent $(NH_3)_n^+$ has the lowest energy barrier for the system. The only common features for the $(NH_3)_n^+$ and $(NH_3BH_3)_n^+$ mass spectra under these conditions are found to be NH_y^+ (y = 0,. . . ,4) at m/z = 14–18. Molecular ions with both ^{11}B and ^{10}B isotopes are observed, and therefore, product ions observed for the $(NH_3BH_3)_n$ cluster system derive from $(NH_3BH_3)_n$ clusters themselves, not from the NH_3 moiety of NH_3BH_3 alone. $NH_3BH_2^+$ is the most abundant ionization product in the $(NH_3BH_3)_n^+$ cluster spectra: calculations support that for $NH_3BH_3^+$, an H atom is lost from the BH_3 moiety with an energy barrier of 0.67 eV. For $(NH_3BH_3)_2^+$ and $(NH_3BH_3)_3^+$ clusters, a $B^{\delta+}\cdots H^{\delta-}\ldots{}^{\delta-}H\cdots{}^{\delta+}B$ bond can form in the respective cluster ions, generating a lower energy, more stable ion structure. The first step in the $(NH_3BH_3)_n^+$ (n = 2, 3) dissociation is the breaking of the $B^{\delta+}\cdots H^{\delta-}\ldots{}^{\delta-}H\cdots{}^{\delta+}B$ moiety, leading to the subsequent release of H_2 from the latter cluster ion. The overall reaction mechanisms calculated are best represented and understood employing a CASSCF natural bond orbital description of the valence electron distribution for the various clusters and monomers. Comparison of the present results with those found for solid NH_3BH_3 suggests that NH_3BH_3 can be a good hydrogen storage material. *Published by AIP Publishing.* [http://dx.doi.org/10.1063/1.4945624]

I. INTRODUCTION

Ammonia borane (NH_3BH_3) is a non-toxic, environmentally friendly, and chemically stable hydrogen storage material for fuel cell power applications; it is safe to use in the air compared to other boron related materials, such as B_2H_6.[1–3] It contains 190 g/kg (19.6 wt. %) hydrogen,[1,2,4,5] is more hydrogen dense than liquid hydrogen, and can be safely stored at normal temperatures and pressures.[6,7]

NH_3BH_3 is isoelectronic with the simple hydrocarbon C_2H_6: it is a crystalline, van der Waals, hydrogen bonded solid at 300 K, and due to the different electronegativities of B and N, ammonia borane is a multi-polar molecule in clusters and the crystal.[2,8] Structures of the NH_3BH_3 crystal, isolated molecule, and small clusters are studied both experimentally and theoretically in previous research work.[9–24] The B–N bond of NH_3BH_3 is formed by the donation of ammonia lone-pair electrons to the empty *p*-orbital of borane. For condensed phase and clusters, each hydridic end (BH) of ammonia borane acts as a hydrogen acceptor for the protic end (NH) of an adjacent molecule:[13,25] the B–N bond between the donor atom and the acceptor atom is considerably shorter in the crystal than it is in a gas phase cluster.[15,18,23,24] The general trend is that shorter bonds are found in larger conglomerates.[24] The shortening of the B–N bond (by ~0.1 Å) in the NH_3BH_3 crystal is directly related to the enhancement of electron donation ($NH_3 \rightarrow BH_3$), as well as electrostatic contributions.[23] In NH_3BH_3 clusters and crystal, neighboring molecules are linked by a network of $N–H^{\delta+}\cdots H^{\delta-}–B$ dihydrogen bonds[13–20,23,26] as is supported by high pressure Raman studies.[26] A dihydrogen bond is an analogue of the conventional hydrogen bond but involves the interaction between a positively charged (protic) hydrogen, bound to an atom of high electronegativity (N–H) and a hydrogen bonded to a less electronegative atom, a hydridic proton (B–H).[8,27,28] Formation of a dihydrogen network appears to be very important, as it leads to substantial stabilization of the single NH_3BH_3 unit.[23] The H· · ·H distance is around 1.7-2.2 Å, which is less than the sum of the van der Waals H atom radii of 2.4 Å:[2,17,28] an average interaction energy of 3 kcal/mol (without zero-point correction) for the dihydrogen bond is

a)Author to whom correspondence should be addressed. Electronic mail: erb@Colostate.edu

predicted,[13,15,23] which shows that these bonds in ammonia borane crystals or clusters are relatively weak. NH_3BH_3 dimer may exhibit two, three, or four equivalent H···H bonds depending on different characterizations suggesting inactions of one N–H hydrogen and two B–H hydrogens of each monomer.[13,14,16,18,20,21,23] At low pressures, the crystalline structure of NH_3BH_3 is stabilized by these charge transfer dihydrogen interactions, while at high pressure, polymorphs are predicted to form layered structures: stacking of layers is determined by an additional homo-polar $B–H^{\delta-}\cdots H^{\delta-}–B$ interaction.[8] The $B–H^{\delta-}\cdots H^{\delta-}–B$ interaction is comparable in bond length to a conventional hydrogen bond: it is the result of a secondary interaction of B–H bonds between monomers with a remarkably short H···H distance of about 2.03 Å.[8,29]

Partial release of hydrogen (6 wt. %) from solid phase NH_3BH_3 occurs at temperatures between 343 and 363 K during long isothermal periods.[3] Upon heating, NH_3BH_3 releases one equivalent of hydrogen (H_2) in each of the three decomposition steps, forming polyaminoborane $(NH_2BH_2)_n$ (90-120 °C), polyiminoborane $(NHBH)_n$ (120-200 °C), and finally boron nitride BN (>500 °C).[4] Decomposition of crystalline NH_3BH_3 near ambient pressure (1039 mbar and 860 mbar) yields intense mass spectral features H_2 ($m/z = 2$) and $m/z = 41$. At pressures lower than 860 mbar, beside the predominate mass spectral fragmentation features at $m/z = 2$ and $m/z = 41$, features at m/z between 78 and 80 (borazine $(BHNH)_3$), m/z between 27 and 29 (aminoborane ($BH_2 = NH_2$)), m/z between 10 and 13, m/z between 23 and 26 (diborane (B_2H_6)), and at $m/z = 42$ (aminodiborane ($BH_2NH_2BH_3$)) are also detected.[3]

Ab initio calculations for the isolated NH_3BH_3 molecule have provided important clues to the reaction pathways leading to the thermal decomposition of NH_3BH_3 forming H_2. In the gas phase, an H atom is transferred from the NH_3 moiety to boron of the same molecule and concomitantly the other two B–H bonds elongate, leading to the formation of H_2 with an activation energy of 32-33 kcal/mol:[21,22] this energy is significantly higher than that expected from the experimental decomposition temperature of about 80 °C.[27] The low temperature experimental rate constant maybe largely influenced by tunneling,[22] which can circumvent this large activation energy barrier. Thermogravimetric analysis of the solid suggests that the N–H···H–B and B–H···H–B fragmentation pathways for an H_2 product contribute nearly equal amounts of hydrogen below 120 °C, with the former becoming dominant after the solid has melted and molecules become mobile.[29] Activation energy for the B–N bond cleavage channel giving rise to NH_3 and BH_3 is 23-26 kcal/mol, so direct B–N dissociation is expected to predominate over H_2 loss.[21,22] Calculations find that an energetically low-lying reaction channel, involving participation of BH_3 as a catalyst for H_2 elimination, also exists.[22] A number of possible dimer structures involving different types of hydrogen bond interactions, and thereby, different fragment atoms and molecules, have been identified through calculations. $(NH_3BH_3)_2$ can generate H_2 via several direct pathways with activation energy barriers ranging from 44 to 50 kcal/mol.[21]

In the present study, a 118 nm laser (10.51 eV/photon, ~10^{12} photons/pulse) is employed as a high energy, single photon ionization source for study of the dynamics and fragmentation of the ammonia borane NH_3BH_3 cation and its cluster ions, through time of flight mass spectrometry (TOFMS). Reactions of hydrogen bonded clusters have received significant attention in the past years.[30–34] Vacuum ultraviolet (VUV) laser radiation can photoionize organic molecules, providing useful dissociation channels.[30,31] Single photon ionization is a good approach for studying van der Waals and hydrogen bonded clusters since less fragmentation of the parent cluster ions occurs compared to electron impact ionization and multi-photon ionization (MPI) with fs or ns lasers.[30–34] Mass spectra of molecules and clusters can provide a window through which to explore fragmentation mechanisms and thermodynamic properties.[31] The potential surfaces for ion decomposition, based on the experimental results, are studied through quantum chemistry calculations.

In order to explicate the ammonia borane results, assign the decomposition products observed in the mass spectra, and to insure the observed reaction products arise from ammonia borane as a whole molecular or cluster ion and not from a fragmented NH_3 moiety, the behavior of ammonia and its clusters is investigated under identical conditions for comparison with $(NH_3BH_3)_n^+$ cation behavior. Additionally, ammonia plays an important role in the chemistry of planetary atmospheres, and its clusters and photochemical products are interesting because they exist in Jovian planets and satellites and will condense into layers of clouds at some tropospheric levels.[35,36] $(NH_3)_n$ neutrals and ions are characterized by van der Waals interactions as are $(NH_3BH_3)_n$ species.[32] Ammonia is a poor proton donor, but a good proton acceptor. With regard to neutral ammonia clusters, the dimer $(NH_3)_2$ is a hydrogen bonded complex with a non-linear H-bond structure, the minimum energy structure of ammonia trimer $(NH_3)_3$ is found to be a cyclic triangle, the ammonia tetramer $(NH_3)_4$ is found to have either a planar ring or cyclic boat structure, and the ammonia pentamer $(NH_3)_5$ is found to have either a distorted pyramid or cyclic ring structure. The larger ammonia clusters (n > 3) have several nearly degenerate conformations, and interconversions among them are facile.[37–44] Structures of nascent unprotonated cluster cations $(NH_3)_n^+$ have been studied as they are the precursors for further decomposition reactions; that is, vertical ionization energy (VIE) > adiabatic ionization energy (AIE).[32–34] $(NH_3)_n^+$ structures are found to have proton transferred type dimer cation cores, $NH_4^+\cdots NH_2$.[45–48] Protonated cluster ions $(NH_3)_nH^+$ are the main fragment arising from photoionized clusters due to intracluster ion molecule reactions and are the most prominent features in the mass spectrum.[45,49–52] For single photon ionization, this reaction is proposed as an absorption/ionization/dissociation (AID) mechanism,

$$(NH_3)_n + h\upsilon \rightarrow [(NH_3)_n^+]^* + e^- \rightarrow (NH_3)_{n-1}H^+ + NH_2 + e^- \text{ (Ref. 52)}.$$

Structures and dynamics of medium sized aggregate ions of ammonia and decomposition mechanisms of $(NH_3)_n^+$ based on the single photon ionization mass spectrometry are studied in this work. Following the ammonia cluster ion studies, structures, molecular orbitals, charge distributions, spin

densities for NH_3BH_3 and its cluster ions are also investigated. Based on assignments of 118 nm photoionization products of ammonia and ammonia borane, potential energy surfaces and dissociation mechanisms are explored theoretically for $NH_3BH_3^+$ and clusters $(NH_3BH_3)_2^+$ and $(NH_3BH_3)_3^+$ through *ab initio* quantum chemistry calculations [complete active space self-consistent field (CASSCF), MP2/6-311++G(d,p)].

II. EXPERIMENTAL PROCEDURES

The experimental setup consists of a supersonic jet expansion nozzle, a 118 nm single photon ionization laser source, and a linear time of flight mass spectrometer (TOFMS): details of the instrumental design are described in our previous papers.[53–56] Briefly, the nozzle used for the molecular beam generation is constructed from a Jordan Co. pulsed valve and a laser desorption source. NH_3BH_3 is purchased from Sigma-Aldrich Co. with 97% purity. The NH_3BH_3 solid sample is put into a copper container inside the pulsed valve behind the nozzle, where the compound is vaporized at 70, 80, and 95 °C. A digital temperature controller within the model REX-C100 nozzle power supply maintains nozzle temperature at 70, 80, and 95 °C. Ammonia borane is entrained into the flow of He carrier gas under a backing pressure of 70 psi through the 2 × 60 mm channel in the laser desorption head and is expanded into the vacuum chamber. For ammonia gas studies, 1% NH_3 in He at a pressure of 70 psi is applied to the nozzle whose temperature is controlled at 25 and 95 °C, to explore the effect of temperature on the observed cluster chemistry. With 70 psi He backing pressure for the closed pulsed valve, the chamber pressure remains 8×10^{-8} torr; with the valve open at 10 Hz, the chamber pressure increases to 8×10^{-7} torr.

The molecular beam passes through a skimmer (1 mm diameter) and is perpendicularly crossed by the 118 nm beam focused to a spot size less than 1 mm in diameter at the ionization point. The ninth harmonic of the seeded Nd:YAG laser (118 nm, third harmonic of 355 nm Nd:YAG laser light) is generated in a 1:10 mixture of Xe/Ar at 260 torr pressure. Sample molecules and clusters absorb a single photon from the 118 nm laser (~10^{12} photons/pulse), ionize, and dissociate in the ionization region between the two extraction plates (4.00 and 3.75 kV) of the TOFMS.

The timing sequence of pulsed nozzle and ionization laser is controlled by time delay generators (SRS DG535). The experiment is run at a repetition rate of 10 Hz. Ion signals in the TOFMS are detected by two micro-channel plates (MCPs): signals are recorded and processed on a personal computer (PC) using an Analog-to-digital Converter (ADC) card (Analog Devices RTI-800) and a boxcar averager (SRS SR250).

III. COMPUTATIONAL METHODS

All calculations are conducted using the Gaussian 09 program. Optimized geometry, charge distributions, orbitals, and spin densities for $(NH_3BH_3)_n$ (n = 1-3) cations are studied through both second-order perturbation theory (MP2) and CASSCF, using the 6-311++G(d,p) basis set. No symmetry restrictions are applied for these calculations. The equilibrium geometry calculations are conducted by taking the total charge as +1 and the spin multiplicity as 2 (S = 1/2) for cations; harmonic frequencies are generated to ensure that no imaginary frequencies are present in the final optimized structures. Charge distribution values are provided using CHELPG (charges from electrostatic potentials employing a grid) based methods and orbitals shown are natural bond orbitals (NBOs).

The critical points on the potential energy surfaces for $(NH_3BH_3)_n^+$ and $(NH_3)_n^+$ ion decomposition processes are explored using MP2/6-311++G(d,p): this approach has been demonstrated to be reasonable based on previous studies[6,9,13,18,20,22,24,37,39,42,45] of these systems. Following single photon absorption, molecules and clusters are ionized to $(NH_3BH_3)_n^+$ or $(NH_3)_n^+$ and dissociation reactions ensue. The VIE, AIE, and the excess energy from the laser are calculated for each $(NH_3BH_3)_n^+$ and $(NH_3)_n^+$ ion observed. A relaxed scan optimization algorithm, as implemented in the Gaussian 09 program suite, is employed to locate transition and intermediate states along reaction pathways. All geometrical parameters except for the specified bond distance reaction coordinate are optimized and electronic energies are monitored as the specified bond is elongated: the structure with peak potential energy is most likely a transition state, and the structure with local potential energy at a minimum is most likely an intermediate state. To verify these conclusions and obtain a more accurate potential energy surface for the transition/intermediate states, the molecular structure provided in the scan is used as the initial structure in the further optimization calculations with the 6-311++G(d,p) basis set. These calculations provide qualitative mechanisms for unimolecular decomposition processes and possible reaction channels for $(NH_3BH_3)_n^+$ (n = 1-3) and $(NH_3)_n^+$ (n = 1-7) cluster ions based on the dissociation mass spectra obtained from the experiments. The proposed reaction pathways, based on the computational results, provide a qualitative interpretation of the observations.

For the CASSCF methods, both active spaces (12,8) and (14,14) are applied as a comparison with MP2 results employing basis set 6-311++G(d,p). All calculation results are compared with previous experimental and theoretical values, as well. The CASSCF active spaces chosen for the calculations are presented in the supplementary material as Figures S1-S4,[57] including CASSCF(12,8) orbitals for NH_3BH_3 (two σ nonbonding orbitals on the BH_3 group, one σ nonbonding orbital on the NH_3 group, one σ nonbonding orbital on the whole system, one σ bonding orbital on the NH_3 group, one π bonding orbital on the whole system, and two π antibonding orbitals on the NH_3 group) and $(NH_3BH_3)_2$ (one σ nonbonding orbital on the BH_3 groups, two σ nonbonding orbitals on the NH_3 groups, three σ nonbonding orbitals on the whole system, and two π antibonding orbitals on the NH_3 groups), CASSCF(11,8) orbitals for $NH_3BH_3^+$ (three σ nonbonding orbitals on the BH_3 group, three σ nonbonding orbitals on the NH_3 groups, and two π antibonding orbitals on the NH_3 groups), and CASSCF(13,14) orbitals for $NH_3BH_3^+$ (one σ nonbonding orbital on the BH_3 group, eight σ nonbonding orbitals on the whole system, one σ bonding orbital on the whole system, three π antibonding orbitals on the NH_3 group,

and one π antibonding orbital on the BH_3 group). Orbitals that are close in energy to the HOMO/LUMO orbitals and are active for the decomposition reactions experimentally observed are selected for the calculations. For the CASSCF(12,8) calculations in this paper, orbitals chosen are mainly from the set HOMO-4 to LUMO+2. Eight is the orbital number limit for analytical frequency calculations within the CASSCF algorithm (Gaussian 09), essential for computation of mechanisms (e.g., potential energy surfaces, intermediates, activated complexes, and products) for observed reactions. As is shown later in Section V B 1, no significant differences are found among molecular structures computed by CASSCF(12,8) and (14,14) methods, thus, a CASSCF(12,8) approach is employed in most cases as our goals are to track and compare results for neutral and ionic monomers to clusters (n = 2, 3) and to explain ion fragmentation and reaction pathways mechanisms for all species.

The Basis set superposition error (BSSE) correction is important for calculation of binding energies, especially of weakly bound (van der Waals and hydrogen bonded) cluster systems; however, the present study focuses on the decomposition potential energy surfaces of cluster cations. In this case, the ΔE values for decomposition reactions only change by ~10% following application of BSSE corrections and the ΔH values are sufficiently close (enthalpy difference <15%) to experimental values without BSSE corrections to be useful for determining reaction open channels and mechanisms.[57–60] Details of ΔE and ΔH comparisons to experimental and higher level calculational results are presented in Table S1 in the supplementary material.[57] As shown in Section V B 1, $(NH_3BH_3)_n^+$ (n = 2, 3) will form a B–H···H–B structure, which renders BSSE corrections inaccurate. Therefore, the BSSE correction is not considered for the present cases.

IV. EXPERIMENTAL RESULTS AND DISCUSSION

A. 118 nm dissociation mass spectra of NH_3 gas expanded at nozzle temperatures 25 and 95 °C

Figures 1(a) and 2(a) display TOF mass spectra of ammonia clusters (m/z > 10) ionized by 118 nm photons at nozzle temperatures 25 and 95 °C, respectively. Figures 1(b)-1(e) and 2(b)-2(e) enlarge Figures 1(a) and 2(a) into smaller mass ranges emphasizing details in the dissociation mass spectra. The blue traces in Figures 1 and 2 are spectra obtained with the nozzle open and the red traces are spectra obtained with the nozzle closed (background for comparison). For m/z < 30, mass signals observed are 14 (N^+), 15 (NH^+), 16 (NH_2^+), 17 (NH_3^+), 18 (NH_4^+), 28 (N_2^+), and 29. The NH_3^+ ion (m/z = 17) is the most intense feature: Figure 2(c) shows that the m/z = 29 feature is from background contamination.

Protonated ammonia clusters $(NH_3)_nH^+$ (n = 2-6), generated from species $(NH_3)_{n+1}^+$, dominate the mass spectra for m/z > 30, consistent with previous studies.[45,49–52] Features at masses for $(NH_3)_n^+$, $(NH_3)_{n-1}NH_2^+$, and $(NH_3)_nH_2^+$ (or $(NH_3)_{n-1}(H_2O)H^+$) are observed as well at 25 °C with intensities about 10 times weaker than those of respective $(NH_3)_nH^+$ assignments. Specifically, $(NH_3)_n^+$ related signals detected at 25 °C are identified at m/z = 32 (O_2^+, from background), 34 ($(NH_3)_2^+$), 35 ($(NH_3)_2H^+$), 51 ($(NH_3)_3^+$), 52 ($(NH_3)_3H^+$), 68 ($(NH_4)_4^+$), 69 ($(NH_4)_4H^+$), 70 ($(NH_3)_4H_2^+$ or $(NH_3)_3(H_2O)H^+$), 86 ($(NH_3)_5H^+$), 87 ($(NH_3)_5H_2^+$ or $(NH_3)_4(H_2O)H^+$), 103 ($(NH_3)_6H^+$), and 104 ($(NH_3)_6H_2^+$ or $(NH_3)_5(H_2O)H^+$). These weak signals become stronger and more mass peaks can be assigned in the spectrum at nozzle temperature 95 °C: in addition to the ions formed at room temperature, mass signals are identified at m/z = 33 ($NH_3NH_2^+$), 36 ($(NH_3)_2H_2^+$ or $NH_3(H_2O)H^+$), 53 ($(NH_3)_3H_2^+$ or $(NH_3)_2(H_2O)H^+$), 67 ($(NH_3)_3NH_2^+$), and 85 ($(NH_3)_5^+$). Thus, increase of nozzle temperature apparently results in an increase in ultimate cluster ion temperature, which enables clusters to overcome additional dissociation energy barriers. Details of the potential surfaces for $(NH_3)_n^+$ ion decomposition will be discussed in Sec. V A 3 dealing with calculated reaction potential energy surfaces. Mass signals at m/z = 36, 53, 70, 87, and 104 can be assigned as $(NH_3)_{n-1}(H_2O)H^+$ or $(NH_3)_nH_2^+$ ions: this distinction is not readily made based on the experimental results alone. Identification of these ions is discussed below through theoretical calculations by comparing the calculated decomposition energy barriers of $(NH_3)_n^+$ cluster cations with the energy stored in the respective cluster cation species.

B. 118 nm dissociation mass spectra of NH_3BH_3 gas expanded at nozzle temperatures 70, 80, and 95 °C

Figures 3-5(a) display TOF mass spectra of $(NH_3BH_3)_n^+$ cluster cations (m/z > 10) ionized by 118 nm photons, at nozzle temperatures 70, 80, and 95 °C, respectively. Figures 5(b)-5(d) expand Figure 5(a) into smaller mass ranges and present details of the cluster cation dissociation mass spectra. The blue traces in these figures are spectra obtained with the nozzle open and the red traces are obtained with the nozzle closed (for background comparison). Despite partial H_2 release (up to 6 wt. %) on heating solid NH_3BH_3 below 100 °C, NH_3BH_3 is still the dominant solid state species in the sample container. The NH_3BH_3 vapor pressure is low at 25 °C and therefore the nozzle is heated (~70 °C) in order to generate a sufficient amount of gas phase sample for detection of clusters and their products.

At nozzle temperature of 70 °C, as shown in Figure 3, the mass spectra signals obtained for the reacting ion system are at m/z = 15 (NH^+), 16 (NH_2^+), 17 (NH_3^+), 18 (NH_4^+), 28 (N_2 and $NH_2{}^{10}BH_2^+$), 29 ($NH_2{}^{11}BH_2^+$, $NH_3{}^{10}BH_2^+$), 30 ($NH_3{}^{11}BH_2^+$, $NH_3{}^{10}BH_3^+$), 31 ($NH_3{}^{11}BH_3^+$), and 44 ($NH_3{}^{11}BH_2{}^{11}BH_3^+$). Isotopic signal m/z = 43 ($NH_3{}^{10}BH_2{}^{11}BH_3^+$ or $NH_3{}^{11}BH_2{}^{10}BH_3^+$) is not observed at 70 °C mainly because its signal is less than 0.1 mV, in this case, too weak to be detected. The feature at m/z = 30 is the most intense peak: based on the natural abundance ratio of boron isotopes ($^{11}B/^{10}B$, 4/1), the fact that intensity of the m/z = 31 ($NH_3{}^{11}BH_3^+$) signal is much lower than that of the m/z = 30 signal, and the feature at m/z = 29 is small, we conclude that the m/z = 30 peak is mainly due to $NH_3{}^{11}BH_2^+$, with a small contribution from $NH_3{}^{10}BH_3^+$ (the intensity of $NH_3{}^{10}BH_3^+$ should be about a quarter of that found for m/z = 31 ($NH_3{}^{11}BH_3^+$)). Since intensity of the

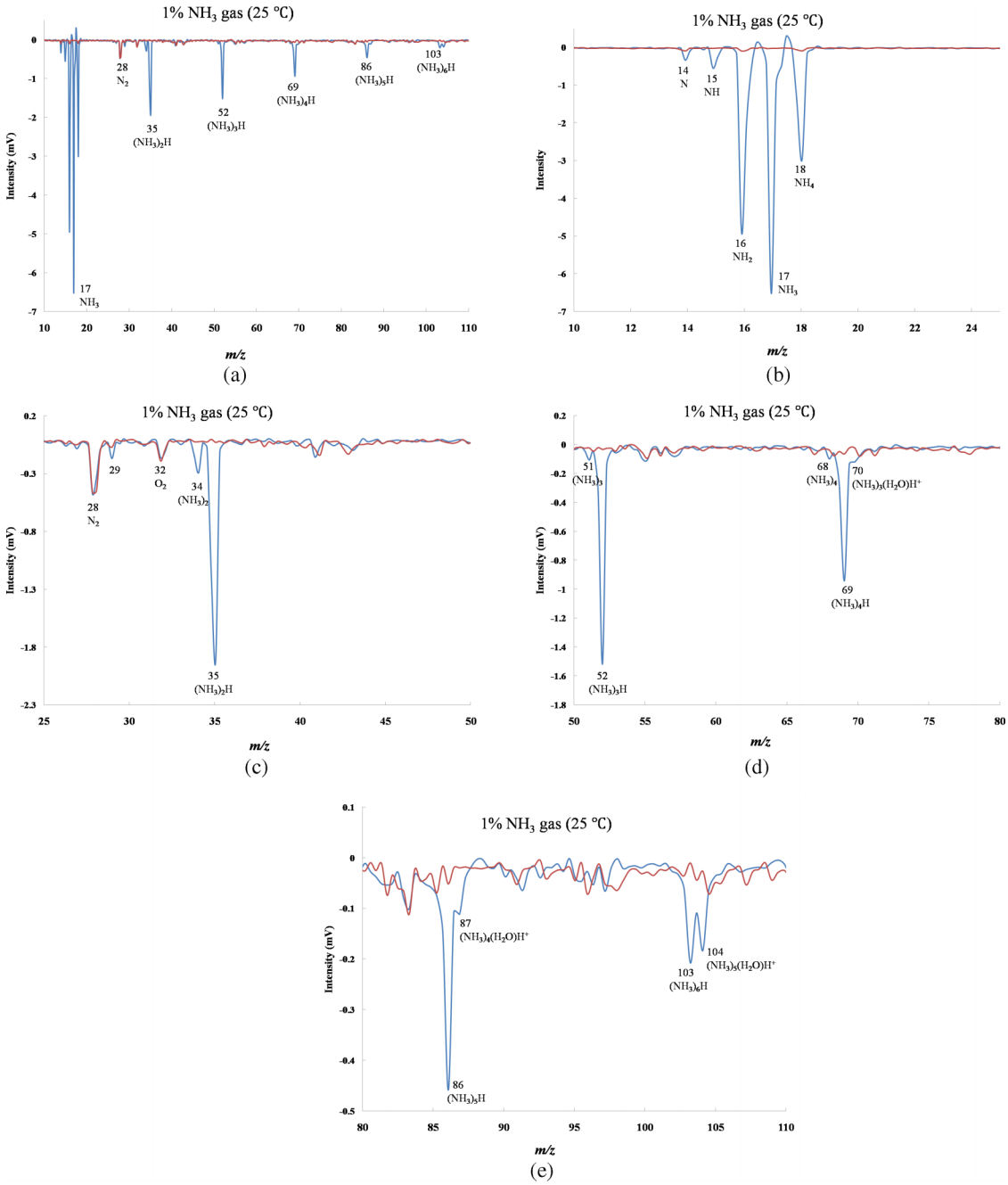

FIG. 1. (a) TOF mass spectrum of 1% NH_3 gas in He ($m/z > 10$) ionized by a 118 nm single photon at nozzle temperature 25 °C. The blue trace is obtained with the nozzle open and the red trace is obtained with the nozzle closed as background for comparison. (b) Mass signals in the range m/z = 10-25 of (a). (c) Mass signals in the range m/z = 25-50 of (a). (d) Mass signals in the range m/z = 50-80 of (a). (e) Mass signals in the range m/z = 80-110 of (a).

signal at $m/z = 29$ is about a quarter of that at $m/z = 30$, we conclude that the $m/z = 29$ feature is dominated by $NH_3{}^{10}BH_2{}^+$, arising from $NH_3{}^{10}BH_3{}^+$ releasing one H atom. The $m/z = 29$ ion can also be $NH_2{}^{11}BH_2{}^+$, $NH_3{}^{11}BH^+$, or $NH^{11}BH_3{}^+$ generated from the loss of H_2 from the nascent $NH_3BH_3{}^+$, but their contribution would be negligible based on the current calculations (Section V B 3), suggesting that loss of H_2 is energetically not feasible. This point is discussed in detail in Section V B 3.

At nozzle temperature of 80 °C, as shown in Figure 4, intensity of the mass signal at $m/z = 44$ ($NH_3{}^{11}BH_2{}^{11}BH_3{}^+$) increases by a factor of 3 compared to its intensity at 70 °C and mass signals at $m/z = 41$ and 43 begin to appear. At nozzle temperature 95 °C, in addition to the features observed at lower temperatures, $m/z = 42$, 72, 73, and 80 peaks are also detected (Figures 5(a)-5(d)). The mass signal $m/z = 30$, although still the most intense one in the spectrum, is about 20% lower compared to its intensity at 70 °C because the NH_3BH_3 solid starts to release H_2 at ~90 °C. Product ions with mass values in the m/z = 41-44 and 78-80 ranges have been observed previously[3] for NH_3BH_3 dehydrogenation reactions. The mass spectral feature at $m/z = 43$ (Figures 5(a) and 5(b)) can be $NH_2{}^{11}BH_2{}^{11}BH_3{}^+$, $NH_3{}^{11}BH^{11}BH_3{}^+$, $NH_3{}^{11}BH_2{}^{11}BH_2{}^+$, $NH_3{}^{11}BH_2{}^{10}BH_3{}^+$, or $NH_3{}^{10}BH_2{}^{11}BH_3{}^+$ (the last two are B isotopic molecules of $m/z = 44$ signal, $NH_3{}^{11}BH_2{}^{11}BH_3{}^+$). From our study of the

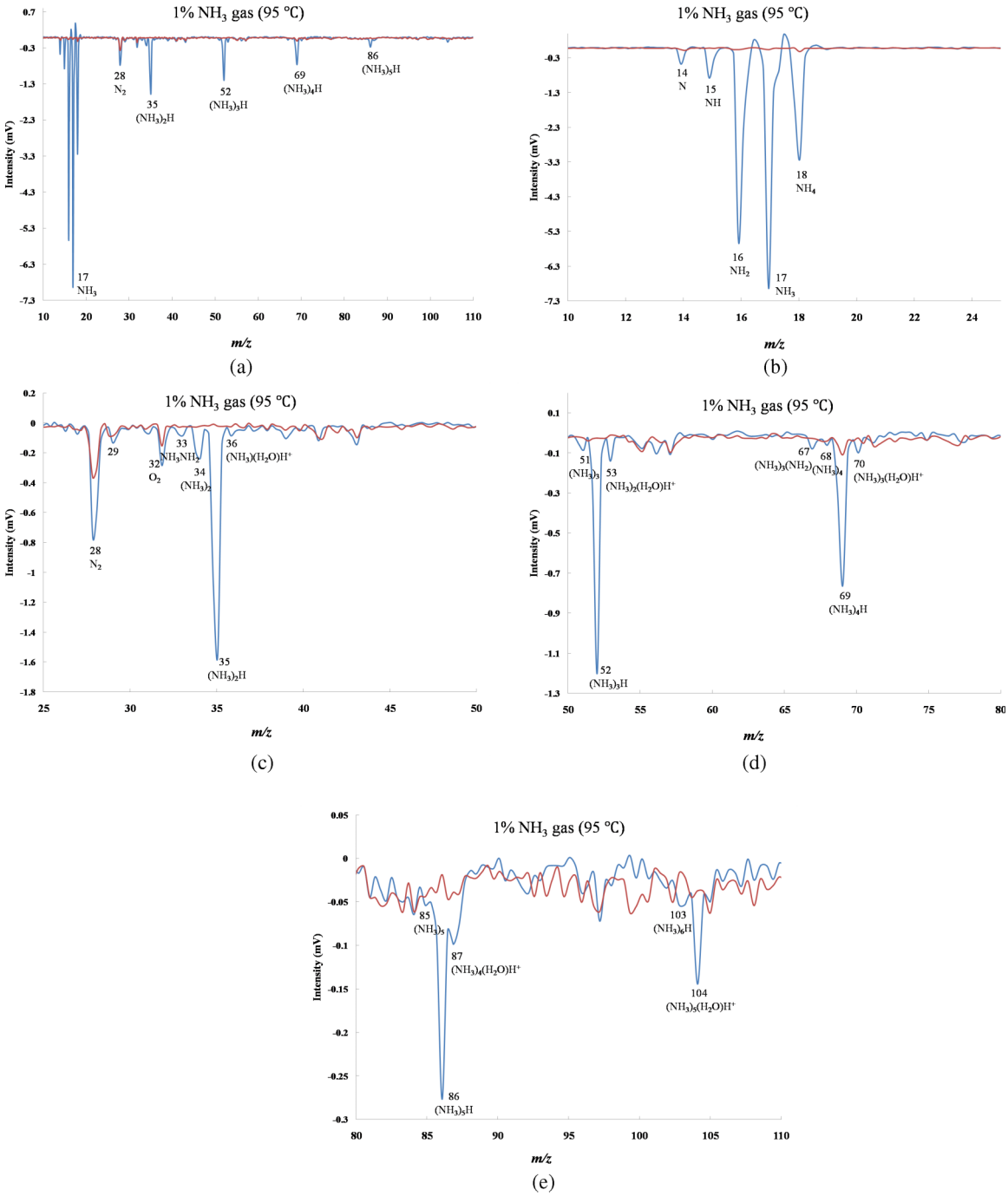

FIG. 2. (a) TOF mass spectrum of 1% NH_3 gas in He ($m/z > 10$) ionized by a 118 nm single photon at nozzle temperature 95 °C. The blue trace is obtained with the nozzle open and the red trace is obtained with the nozzle closed as background for comparison. (b) Mass signals in the range m/z = 10-25 of (a). (c) Mass signals in the range m/z = 25-50 of (a). (d) Mass signals in the range m/z = 50-80 of (a). (e) Mass signals in the range m/z = 80-110 of (a).

cluster cation decomposition mechanisms, $NH_3{}^{11}BH_2{}^{10}BH_3$ or $NH_3{}^{10}BH_2{}^{11}BH_3$ is the primary species contributing to the $m/z = 43$ signal. With two B atoms in this fragment, the isotopic intensity ratio for 44/43 m/z features ($^{11}B^{11}B/^{11}B^{10}B$) becomes 2/1. The $m/z = 43$ signal intensity is higher than half of the $m/z = 44$ signal intensity mainly because of the possible presence of $NH_2{}^{11}BH_2{}^{11}BH_3{}^+$. $NH_2{}^{11}BH_2{}^{11}BH_3{}^+$ ($m/z = 43$) can readily lose an H_2 molecule, forming an $m/z = 41$ product ($NH_2{}^{11}BH^{11}BH_2$). The $NH_3{}^{11}BH_2{}^{11}BH_3$ signal ($m/z = 44$) can form an $m/z = 42$ product $NH_3{}^{11}BH^{11}BH_2$; however, this reaction has a much higher energy barrier compared to the laser limit. Details of these and other dissociation mechanisms are presented in Section V B 3. Therefore, the main contribution of $m/z = 42$ is from either the NH_3BH_3 solid heated at 95 °C or from the B isotopic molecules of $m/z = 43$ and 44 signals: $N^{10}B_2H_8$ and $N^{11}B^{10}BH_7$. Besides $NH_2{}^{11}BH^{11}BH_2$, $m/z = 41$ can be the B isotopic productions of $m/z = 42$ and 43 signals: $N^{10}B_2H_7$ and $N^{11}B^{10}BH_6$. The B isotopic ion of the $m/z = 41$ signal is too weak to be identified in the spectra. The molecular fragment with $m/z = 80$ is $(NH_3{}^{11}BH_3)_2NH_4{}^+$, assigned based on our calculated decomposition mechanisms: B isotopic molecular

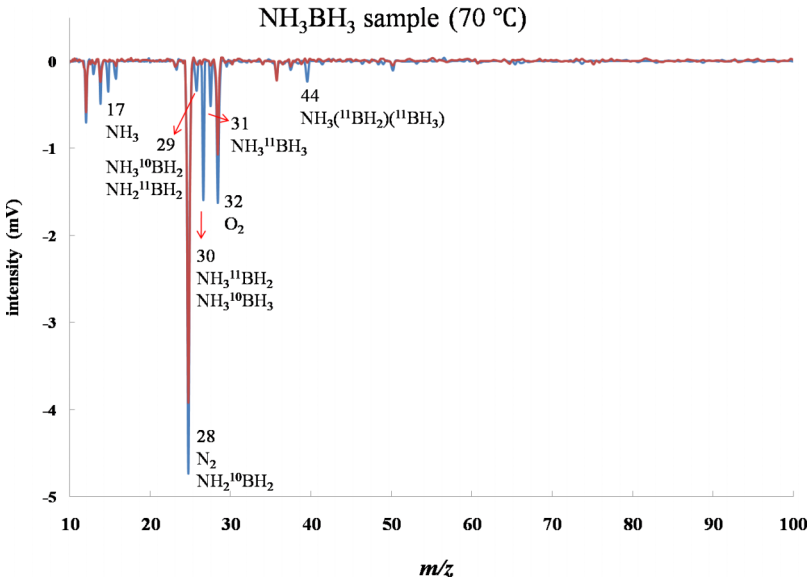

FIG. 3. TOF mass spectrum of $(NH_3BH_3)_n^+$ cluster cations (n = 1-3, $m/z > 10$) ionized by a 118 nm single photon at nozzle temperature 70 °C. The blue trace is obtained with the nozzle open and the red trace is obtained with the nozzle closed as background for comparison.

fragments are too weak to be observed in this instance. The $m/z = 73$ signal can be $(NH_2{}^{11}BH_2)$ $(NH_3{}^{11}BH_2{}^{11}BH_3)^+$: thereby, the $m/z = 72$ feature is most likely its isotopic species $(NH_2{}^{10}BH_2)$ $(NH_3{}^{11}BH_2{}^{11}BH_3)^+$, $(NH_2{}^{10}BH_2)$ $(NH_3{}^{11}BH_2{}^{11}BH_3)^+$, and $(NH_2{}^{10}BH_2)(NH_3{}^{11}BH_2{}^{11}BH_3)^+$. Additionally, the feature at $m/z = 72$ may be formed by $m/z = 73$ $((NH_2{}^{11}BH_2)(NH_3{}^{11}BH_2{}^{11}BH_3)^+)$ dissociating a single H atom. The $m/z = 72$ and 73 signals can also be formed during the nozzle heating process, not through photon dissociation. Details of the decomposition mechanisms for species in the latter m/z range will be discussed in Section V B 3.

As the nozzle temperature increases from 70 to 80 °C, signals at $m/z = 41$ and 43 start to appear. As the nozzle temperature continue to rise to 95 °C, signals $m/z = 42$, 72, 73, and 80 are observed in the mass spectra. The different mass signals found at different nozzle temperatures mainly occur for two reasons. First, as the nozzle is heated to higher temperatures, the NH_3BH_3 vapor pressure increases, and thus, more $(NH_3BH_3)_n$ will flow with the He beam into the laser ionization region. The signal intensities will increase and some weak signals will become detectable through TOFMS. Second, NH_3BH_3 crystal starts to release H_2 slowly at 70 °C and as the temperature increases to 95 °C, more fragments will be dissociated in the nozzle during the heating process, and will be carried by the He beam to the laser ionization region. Whether the fragmentation species are produced by the nozzle heating or by laser dissociation will be discussed in more detail in Section V B 3.

C. Comparison of NH_3 gas and NH_3BH_3 sample mass spectra at 95 °C

To get a better understanding of the $(NH_3BH_3)_n^+$ decomposition mechanisms and to confirm if the decomposition products observed for NH_3BH_3 mass spectra are generated from $(NH_3BH_3)_n$ cluster ions and not simply combinations of NH_3 moieties, single photon dissociation reactions for both ammonia gas and NH_3BH_3 solid samples are obtained under the same conditions for comparison. A number of differences between these two spectra are readily identified. First, the

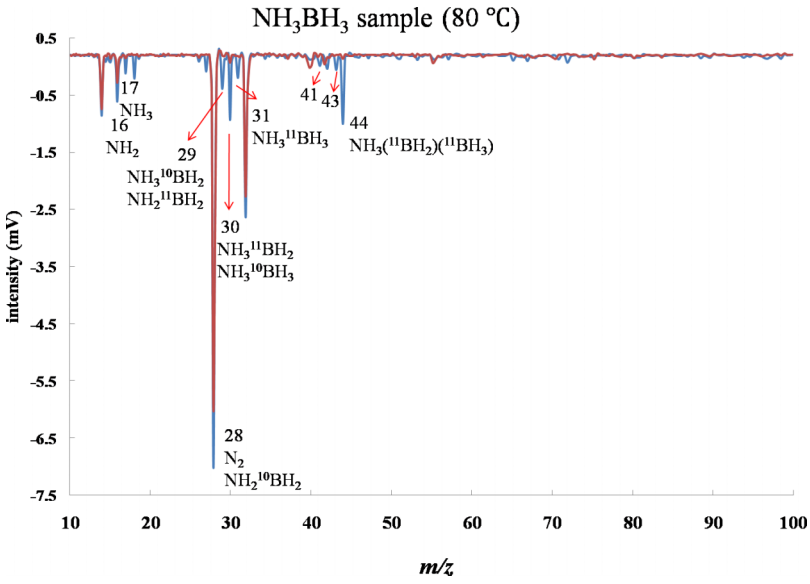

FIG. 4. TOF mass spectrum of $(NH_3BH_3)_n^+$ cluster cations (n = 1-3, $m/z > 10$) ionized by a 118 nm single photon at nozzle temperature 80 °C. The blue trace is obtained with the nozzle open and the red trace is obtained with the nozzle closed as background for comparison.

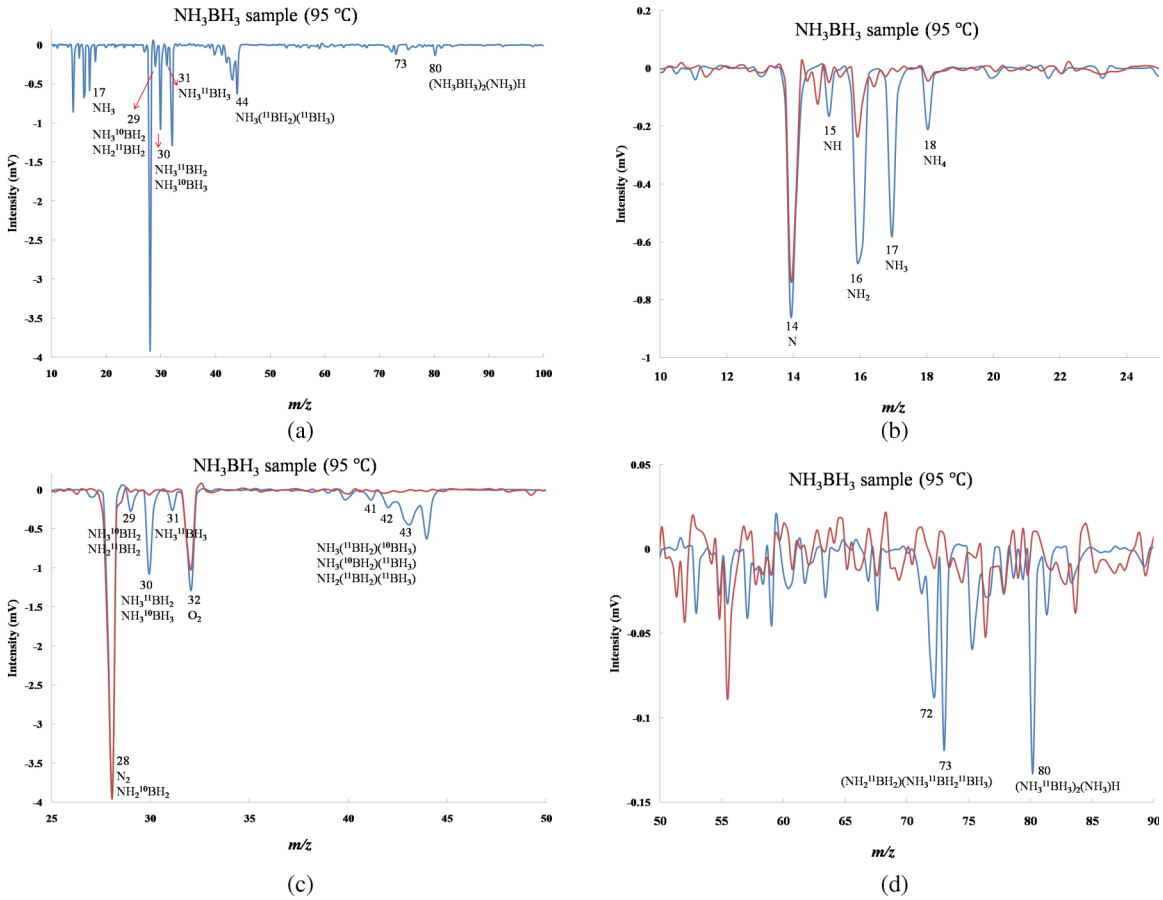

FIG. 5. (a) TOF mass spectrum of $(NH_3BH_3)_n^+$ cluster cations (n = 1-3, $m/z > 10$) ionized by a 118 nm single photon at nozzle temperature 95 °C. The blue trace is obtained with the nozzle open and the red trace is obtained with the nozzle closed as background for comparison. (b) Mass signals in the range m/z = 10-25 of (a). (c) Mass signals in the range m/z = 25-50 of (a). (d) Mass signals in the range m/z = 50-90 of (a).

m/z = 17 (NH_3^+) feature is the most intense signal in ammonia gas mass spectra, while for NH_3BH_3, the NH_3^+ ion signal is much weaker and the peak at m/z = 16 (NH_2^+) is more intense than that at 17. Therefore, $(NH_3BH_3)_n^+$ and $(NH_3)_n^+$ have different mechanisms by which to form NH_n^+ (n = 0-4) ions in single photon ionization/decomposition reactions. Second, the most intense signal in the NH_3BH_3 mass spectrum is at m/z = 30 ($NH_3{}^{11}BH_2^+$), while in the ammonia gas spectrum, no ion signals are observed in the m/z = 29-31 range. Third, other than the NH_n^+ (n = 0-4) ions, the two mass spectra do not share any common ion signals in higher mass ranges, which implies that $(NH_3BH_3)_n^+$ species decomposition products are generated from $(NH_3BH_3)_n^+$ cluster ions, not from fragmented NH_3 species, contaminants in the vacuum chamber, or from polymerization reactions of fragmented $(NH_x)_y$.

V. THEORETICAL RESULTS AND DISCUSSION

A. Structures, ionization, and available decomposition pathways for $(NH_3)_n^+$ cluster ions

1. Structures of neutral and ionic $(NH_3)_n$ clusters

Figure 6 shows the optimized (adiabatic) structures of neutral $(NH_3)_n$ and $(NH_3)_n^+$ cations (n = 2-7). The optimized Cartesian x, y, z coordinates of $(NH_3)_n$ and $(NH_3)_n^+$ (n = 1-7) are summarized in the supplementary material, Table S2.[57] From previous studies, the neutral ammonia dimer is found to have two structures, separated in energy by 0.01 eV.[37] Our results agree with this conclusion: for the 'asym,' lower energy structure (Figure 6), the distances between nitrogen and hydrogen atoms in the H-bond structure N–H···N are 1.018 Å and 2.262 Å, respectively. The neutral ammonia trimer has a cyclic planar triangular (N atom) structure: three hydrogen bonds are formed, with each ammonia molecule acting simultaneously as an H atom donor and acceptor. The distances between nitrogen and hydrogen atoms in these H-bond structures N–H···N are 1.021 Å and 2.217-2.218 Å, respectively. Larger neutral clusters have several nearly degenerate conformations that can undergo interconversion due to low barriers. The most stable isomers for ammonia tetramer, pentamer, hexamer, and heptamer obtained at our calculation level (for N atoms) have a quadrilateral planar cyclic ring, a non-planar five-member cyclic ring, a distorted bi-pyramid, and a complicated three-dimensional global minimum structure, respectively. Analogous to neutral ammonia dimer and trimer structures, hydrogen bonds are formed in the larger clusters: the distances among nitrogen and hydrogen atoms in the H-bond structures N–H···N are summarized in Table I. As neutral cluster size increases, covalent N–H bonds become longer and the hydrogen bond lengths between N and H atoms become shorter. Thus,

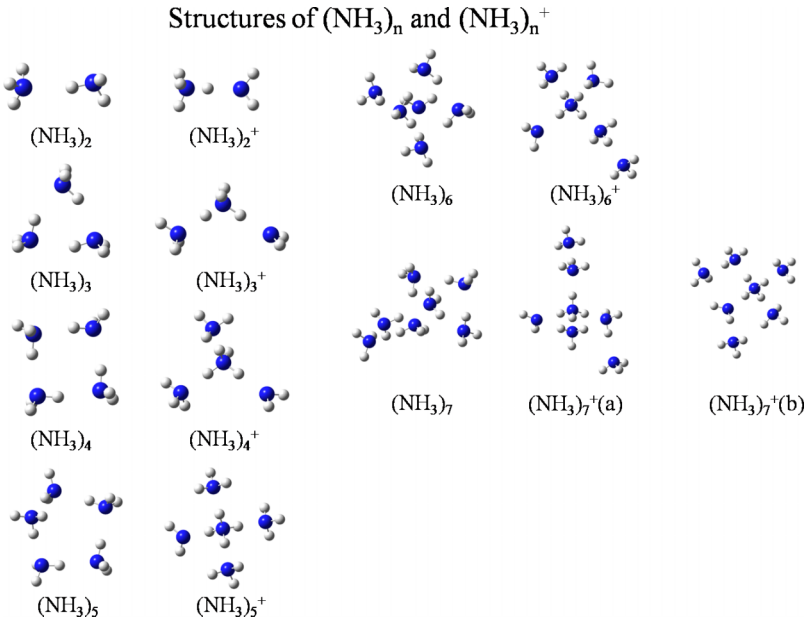

FIG. 6. Optimized adiabatic structures of neutral $(NH_3)_n$ clusters and $(NH_3)_n^+$ cations (n = 2-7) at the MP2/6-311++G(d,p) level. The obtained $(NH_3)_n^+$ structures are called $S_{ion,min}$ later in the paper. $(NH_3)_7^+$ cation has two stable structures (a) and (b): the energy of (a) is 0.04 eV higher than that of (b). For atoms in the structure, blue is nitrogen and grey is hydrogen.

TABLE I. Distances of N and H atoms in H-bond structure N–H···N for neutral $(NH_3)_n$ and distance between N and H atoms in the H_3 N–H···NH_2 charge transferred core for $(NH_3)_n^+$ ions. (Structures shown in Figure 6). The calculation level is MP2/6-311++G(d,p).

	Distances between N and H atoms in H-bond structure N–H···N for neutral $(NH_3)_n$ D(N–H)/D(H···N) (Å)		Distances between N and H atoms in H_3N–H··· NH_2 charge transferred core for $(NH_3)_n^+$ ions $S_{ion,min}$ D(N–H)/D(H···N) (Å)
NH_3	1.013	NH_3^+	...
$(NH_3)_2$	1.018/2.262	$(NH_3)_2^+$	1.074/1.692
$(NH_3)_3$	1.021/2.217-2.218	$(NH_3)_3^+$	1.074/1.717
$(NH_3)_4$	1.024/2.149	$(NH_3)_4^+$	1.038/1.912
$(NH_3)_5$	1.024/2.132-2.151	$(NH_3)_5^+$	1.032/1.979
$(NH_3)_6$	1.024/2.132-2.236	$(NH_3)_6^+$	1.030/2.001
$(NH_3)_7$	1.022-1.027/2.074-2.237	$(NH_3)_7^+$	(a) 1.029/2.019 (b) 1.037/1.911

the interactions among ammonia molecules in the form of hydrogen bonds increase in larger neutral ammonia clusters.

For unprotonated ammonia cluster cations $(NH_3)_n^+$, $NH_4^+\cdots NH_2$ type of structures are predicted. Based on previous IR studies,[46,47] $(NH_3)_2^+$ is unequivocally determined to have a proton transferred structure. Structures of larger clusters (n > 2) can be characterized as a dimer cation core ($NH_4^+\cdots NH_2$) solvated by neutral ammonia molecules. The structure of $(NH_3)_4^+$ is of the same proton transferred type with some energy degenerate isomers. The most stable structures of unprotonated ammonia ions $(NH_3)_n^+$ are also shown in Figure 6. The distances between NH_4^+ and NH_2 moieties in the H_3N–H···NH_2 proton transferred core for each $(NH_3)_n^+$ ion are listed in Table I. Unlike the situation for neutral ammonia clusters, the hydrogen bond distance in the H_3N–H···NH_2 cation structure increases as cluster number increases from 1.692 Å to 2.019 Å (n = 2-7) except for $(NH_3)_7^+$ cation (b) (Figure 6), which forms additional H-bonds between the NH_2 group in the $NH_4^+\cdots NH_2$ core and a nearby NH_3 molecule. This observation suggests that larger ammonia cluster ions can more readily dissociate into smaller moieties than can smaller ones.

2. Ionization energy of $(NH_3)_n$ neutral clusters and the formation of unprotonated $(NH_3)_n^+$ cations with $NH_4^+\cdots NH_2$ core structures

The VIE of each ammonia neutral cluster $(NH_3)_n$ is listed in Table II. The ionization energy decreases from 10.57 eV to 9.20 eV as cluster number n increases from n = 1 to 5. For the hexamer and heptamer, the ionization energy remains at 9.71–9.72 eV. Since energy of the 118 nm laser photon is 10.51 eV, neutral $(NH_3)_n$ clusters are ionized by single photon absorption and photon energy above the VIE is carried away by the exiting photoelectron from the cluster ions as electron kinetic energy.

Our MP2/6-311++G(d,p) and CASSCF(12,8)/6-311++G(d,p) results compared to the previous experimental values are summarized in Table II. The MP2 results overestimate the VIE by about 0.40–1.12 eV, while the CASSCF results are closer to the experimental values; however, all the calculated vertical ionization energies are acceptable for the present work.

When an ammonia cluster is ionized, as shown in Figure 7, it evolves to a more stable ion structure $S_{ion,min}$ with an ionic

TABLE II. Vertical ionization energy (VIE), adiabatic ionization energy (AIE), energy stored in the ion system (ΔE) calculated in MP2/6-311++G(d,p) and CASSCF(12,8)/6-311++G(d,p) methods and compared with previous experimental studies.

	MP2 (eV)			CASSCF(12,8) (eV)	Exp (eV)[a,b,c]
	VIE	AIE	ΔE	VIE	VIE
NH_3	10.57	9.88	0.69	9.93	10.17
$(NH_3)_2$	10.40	8.54	1.86	8.86	9.54 ± 0.05
$(NH_3)_3$	9.81	7.69	2.12	9.00	9.3
$(NH_3)_4$	9.36	7.24	2.12	8.70	9.0
$(NH_3)_5$	9.20	6.83	2.37		8.7
$(NH_3)_6$	9.72	6.74	2.98		8.6
$(NH_3)_7$	9.71	6.56	3.15		...

[a]Reference 61.
[b]Reference 62.
[c]Reference 63.

$NH_4^+\cdots NH_2$ core, as mentioned above (structures of $S_{ion,min}$ are shown in Figure 6), within ca. 100 fs or less. The energy difference between ammonia neutral cluster and the ground state unprotonated cation structure with a $NH_4^+\cdots NH_2$ core is the AIE of $(NH_3)_n^+$ ions (Table II). The AIE value decreases from 9.88 eV to 6.56 eV as cluster size increases from n = 1 to 7. For $(NH_3)_2^+$, from previous studies,[37,39,42,47] $S_{ion,min}$ can be formed through intra-cluster proton or hydrogen atom transfer after vertical ionization without an effective energy barrier. Our calculations agree with these conclusions: the AIE value for $(NH_3)_2^+$ is 8.54 eV, 1.86 eV lower than its VIE and this 1.86 eV energy is stored in the ion system as vibrational energy, available for dissociation reactions and additional rearrangements.

For $(NH_3)_n^+$ (n > 2), stable adiabatic ion structures $S_{ion,min}$ can be formed through intra-cluster proton or hydrogen atom transfer following 118 nm photoionization of $(NH_3)_n$. As shown in Figure 7, our calculation provides one of the possible reaction pathways forming the adiabatic $(NH_3)_n^+$ cation $S_{ion,min}$. For example, following ionization, $(NH_3)_3^+$ will form a triangle ring structure for heavy atoms $S_{ion,im}$ first that is close to the Frank Condon structure $S_{ion,FC}$ of neutral $(NH_3)_3$. The energy of this intermediate $S_{ion,im}$ is 9.44 eV, 0.37 eV lower than the VIE. Next, the triangle ring of $S_{ion,im}$ opens after surmounting a small energy barrier of 0.35 eV. The energy of this transition state $S_{ion,ts}$ is 9.79 eV: lower in energy than the VIE, and a proton or H atom transfer reaction can occur following the ring opening reaction. The energy of the core transferred adiabatic structure $S_{ion,min}$ for $(NH_3)_3^+$ is 7.69 eV; therefore, the energy stored in the ion system for dissociation reactions is 2.12 eV. The energy differences between VIE and AIE for $(NH_3)_n^+$ (n = 1-7) ions are ΔE (Figure 7 and Table II). As cluster size increases, energy stored (ΔE) in the cluster ion system for dissociation reactions and further rearrangements increases.

3. Decomposition mechanisms for $(NH_3)_n^+$ cluster ions

The detailed dissociation potential energy surfaces for $(NH_3)_n^+$ cluster ions are shown in Figures 8-13. Taking $(NH_3)_3^+$ as an example (Figure 9), when the core transferred

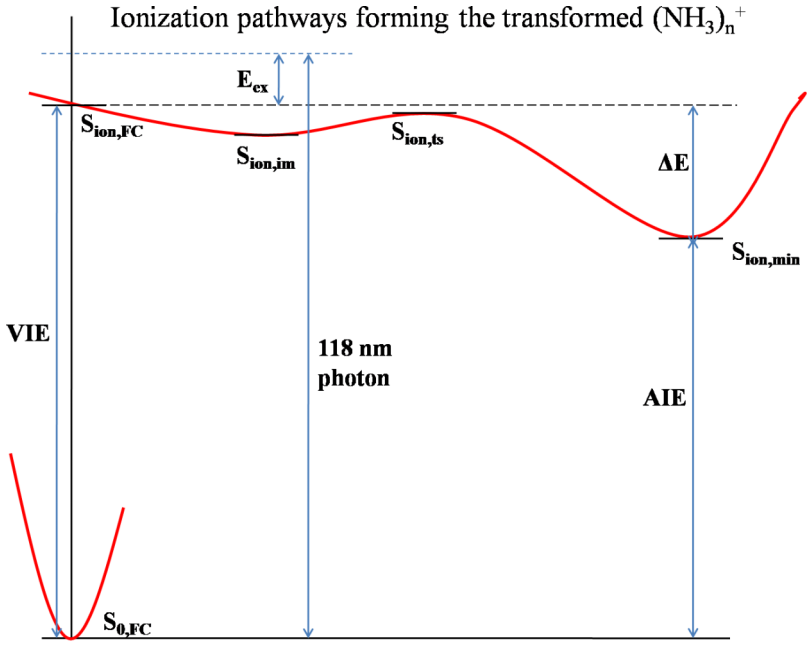

FIG. 7. Ionization pathways forming the transformed $(NH_3)_n^+$ cation. $S_{ion,FC}$ is the Frank Condon structure of neutral $(NH_3)_n$, $S_{ion,im}$ is a intermediate state, $S_{ion,ts}$ is the transition state for the ring open of $S_{ion,im}$, and $S_{ion,min}$ is the optimized adiabatic structure of $(NH_3)_n^+$. VIE is vertical ionization energy, AIE is adiabatic ionization energy, ΔE is the energy stored in the $(NH_3)_n^+$ system for further dissociation reaction, and E_{ex} is the excess energy taken away by photon electron.

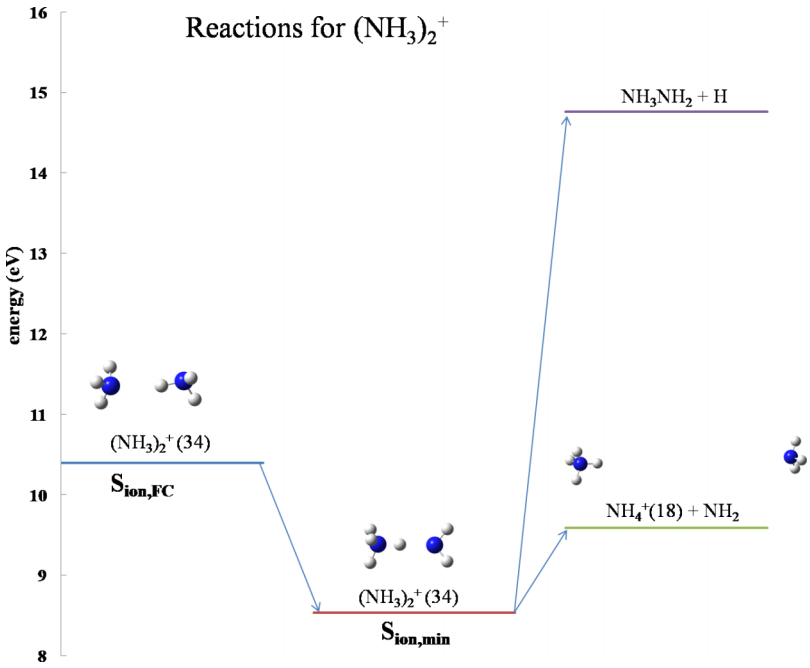

FIG. 8. The detailed dissociation potential surface for $(NH_3)_2^+$. Mass signal NH_4^+ (18) observed in the experiment can be formed within the energy limit based on the calculations. For atoms in the structure, blue is nitrogen and grey is hydrogen. The calculation level is MP2/6-311++G(d,p).

ion structure $S_{ion,min}$ is formed, three possible fragmentation pathways are calculated. First, NH_2 is released from the system producing the protonated cluster cation $(NH_3)_2H^+$. The energy barrier for this reaction is 0.70 eV, which is the smallest among all three dissociation reactions, and it is energetically feasible (Table II). $(NH_3)_nH^+$ has the most intense mass signals in the ammonia gas mass spectra, and thus, this theoretical result is consistent with the experimental observations. Second, an H atom is released producing $(NH_3)_2NH_2^+$ with energy barrier 2.82 eV, which is higher than the available ΔE. Though release of a single H atom is energetically unfavorable, when combined with an ammonia molecule, the energy barrier is much lower. The energy barrier for $(NH_3)_3^+$ releasing an NH_4 moiety forming $NH_3NH_2^+$ is 1.72 eV, close to the energy limit ΔE stored in this system. Based on the experimental weak $(NH_3)_nNH_2^+$ signals, calculations show that these latter clusters can be produced by $(NH_3)_{n+1}^+$ cations releasing an NH_4 moiety. Third, the protonated ion product $(NH_3)_nH^+$ can release an additional NH_3 neutral molecule forming $(NH_3)_{n-1}H^+$. In the $(NH_3)_3^+$ ion system, this energy barrier is 1.91 eV, close to the energy limit ΔE.

As ammonia cluster size increases, the energy barriers for creating product ions decrease, as shown in Figures 10-13. The three types of fragmentation reactions enumerated above are considered for all $(NH_3)_n^+$ (n = 2-7) cluster cations. The $(NH_3)_7^+$ cluster cation in this series is different from the others: two stable transferred $(NH_3)_7^+$ core structures $S_{ion,min}$ (a) and (b), which differ in energy by 0.04 eV (see Figure 6), are

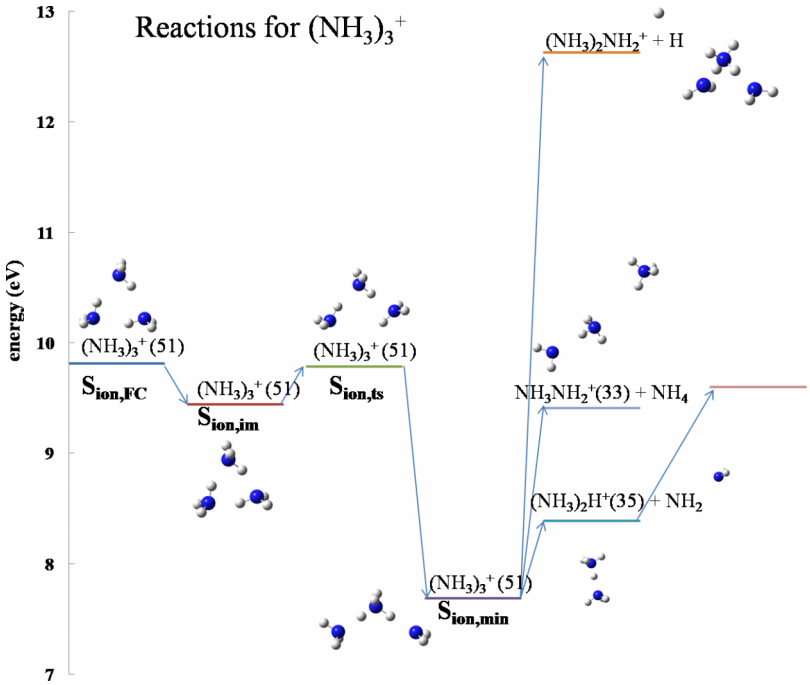

FIG. 9. The detailed dissociation potential surface for $(NH_3)_3^+$. Mass signals $(NH_3)_2H^+$ (35), $NH_3NH_2^+$ (33), and NH_4^+ (18) observed in the experiment can be formed within the energy limit based on the calculations. For atoms in the structure, blue is nitrogen and grey is hydrogen. The calculation level is MP2/6-311++G(d,p).

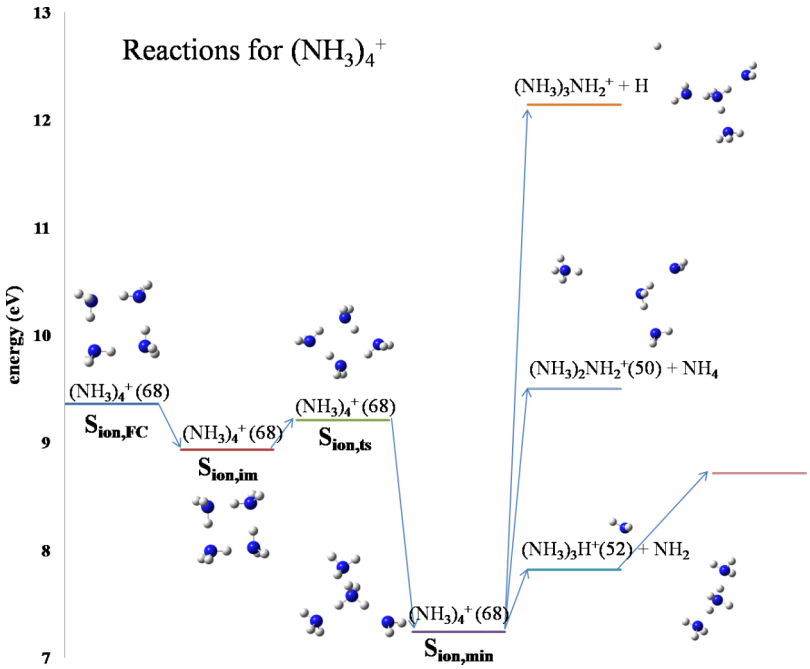

FIG. 10. The detailed dissociation potential surface for $(NH_3)_4^+$. Mass signals $(NH_3)_3H^+$ (52) and $(NH_3)_2H^+$ (35) observed in the experiment can be formed within the energy limit based on the calculations. $(NH_3)_2NH_2^+$ (50) formation is 0.14 eV above the VIE. For atoms in the structure, blue is nitrogen and grey is hydrogen. The calculation level is MP2/6-311++G(d,p).

located. Both structures are most likely present for the $(NH_3)_7^+$ system: one dissociates to form $(NH_3)_6H^+ + NH_2$ product and the other dissociates to form $(NH_3)_5H^+ + NH_3 + NH_2$ products (Figure 13). Their pathways have similar energy barriers of 0.45 eV and 0.63 eV, respectively.

Based on the ammonia cluster mass spectra, ion signals at $m/z = 36$, 53, 70, 87, and 104 are related to either $(NH_3)_nH_2^+$ ions or H_2O contaminated $(NH_3)_{n-1}(H_2O)H^+$ ions. The latter species may be adducts of ammonia and outgassed water contaminant in the manifold behind the pulsed nozzle. To determine assignments of these features, several other fragmentation pathways for $(NH_3)_n^+$ must be considered. The energy barrier for $(NH_3)_5^+$ dissociation reaction $(NH_3)_5^+ \rightarrow (NH_3)_2H_2^+$ (36) + $(NH_3)_2NH$ (Figure 11, red dashed line) is 2.91 eV higher than the VIE, which makes this type of reaction unfavorable. For $(NH_3)_6^+$, the energy barrier of reaction $(NH_3)_6^+ \rightarrow (NH_3)_3H_2^+$ (53) + $(NH_3)_2NH$, as shown in Figure 12 for the red dashed line, is 1.32 eV higher than the energy limit. Two decomposition reactions for the $(NH_3)_7^+$ system, $(NH_3)_7^+ \rightarrow (NH_3)_4H_2^+$ (70) + $(NH_3)_2NH$ and $(NH_3)_7^+ \rightarrow (NH_3)_5H_2^+$ (87) + $(NH_3)_2NH$ (Figure 13, red dashed lines), are studied. The energy barrier for the former reaction is 0.94 eV higher than the limit, while the energy barrier of the latter is 0.23 eV higher than the energy limit for this cluster ion system. As the number of ammonia molecules in a cluster increases, the energy barriers for $(NH_3)_n^+$ fragmentation creating $(NH_3)_{n-1}H_2^+$ products decrease. This type of reaction may be possible in larger ammonia clusters. Nonetheless, detection of signals $(NH_3)_nH_2^+$ (n = 2-7), but not $(NH_3)_nH^+$ (n > 7) signals, is not readily explicable. Therefore, we suggest that mass signals at m/z = 36, 53, 70, 87, and 104 are most likely hydrated ions $(NH_3)_{n-1}(H_2O)H^+$, which are

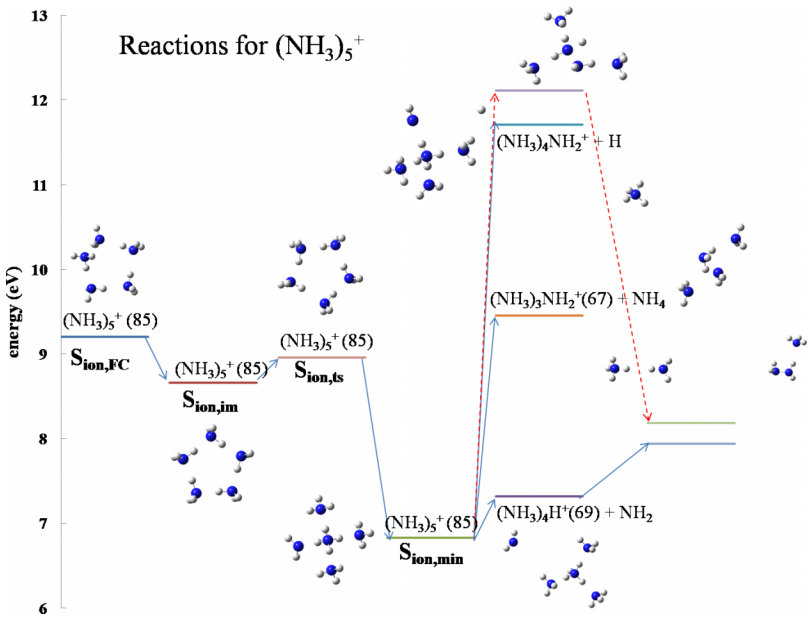

FIG. 11. The detailed dissociation potential surface for $(NH_3)_5^+$. Mass signals $(NH_3)_4H^+$ (69) and $(NH_3)_3H^+$ (52) observed in the experiment can be formed within the energy limit based on the calculations. $(NH_3)_3NH_2^+$ (67) formation is 0.25 eV above the VIE. For atoms in the structure, blue is nitrogen and grey is hydrogen. The calculation level is MP2/6-311++G(d,p).

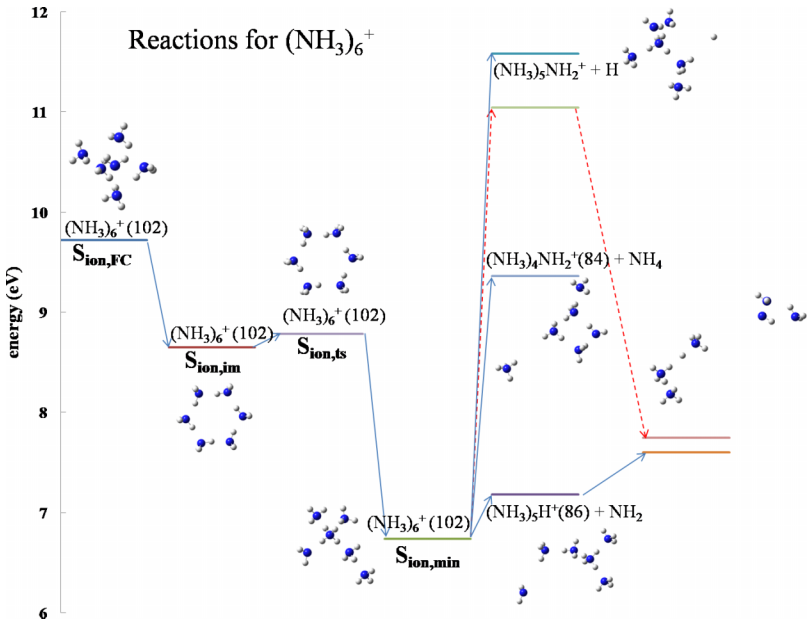

FIG. 12. The detailed dissociation potential surface for $(NH_3)_6^+$. Mass signals $(NH_3)_5H^+$ (86), $(NH_3)_4NH_2^+$ (84), and $(NH_3)_4H^+$ (69) observed in the experiment can be formed within the energy limit based on the calculations. For atoms in the structure, blue is nitrogen and grey is hydrogen. The calculation level is MP2/6-311++G(d,p).

formed through a similar mechanism to that in Equation (1) below. At nozzle temperatures ~95 °C, the intensities of these mass signals increase because more water vapor (probably from outgassing) is present in the nozzle system than at lower temperatures.

The ammonia cluster cations $(NH_3)_n^+$ decomposition reactions can be summarized as

$$(NH_3)_n^+ \rightarrow (NH_3)_{n-1}H^+ + NH_2 \quad (1)$$

$$(NH_3)_n^+ \rightarrow (NH_3)_{n-2}NH_2^+ + NH_4 \quad (2)$$

$$(NH_3)_{n-1}H^+ \rightarrow (NH_3)_{n-2}H^+ + NH_3. \quad (3)$$

Energy barriers for $(NH_3)_n^+$ (n = 2-7) fragmentation reactions producing $(NH_3)_{n-1}H^+$, $(NH_3)_{n-1}NH_2^+$, $(NH_3)_{n-2}H^+$ products in reactions (1)-(3) are summarized in Table III. Reaction (1) has the lowest energy barrier, which decreases from 1.05 eV to 0.22 eV as the cluster size increases. The energy barrier for Equation (2) is close to the energy limit ΔE in the cation system, and for reaction (3), similar to reaction (1), the energy barriers decrease from 1.91 eV to 0.63 eV as the cluster size increases. $(NH_3)_{n-1}H^+$ cations created through Equation (1) with mass signals at m/z = 35, 52, 69, 86, and 103 are the dominant dissociation products in the $(NH_3)_n^+$ mass spectra. At nozzle temperature ~25 °C, ion products $(NH_3)_{n-2}NH_2^+$ from reaction (2) are barely observed in the mass spectra, as shown in Figure 1. As the temperature is increased to 95 °C, ion signals with m/z = 33 ($NH_3NH_2^+$) and 67 ($(NH_3)_3NH_2^+$) begin to appear. Calculations show that the energy barriers forming $(NH_3)_nNH_2^+$ ions are very close to the energy limit ΔE in the reaction systems; therefore, nozzle heating assists $(NH_3)_n^+$ to overcome these reaction barriers.

In summary, the most stable calculated structures for neutral ammonia clusters are consistent with results from previous studies. Their cations $(NH_3)_n^+$ have a proton or H

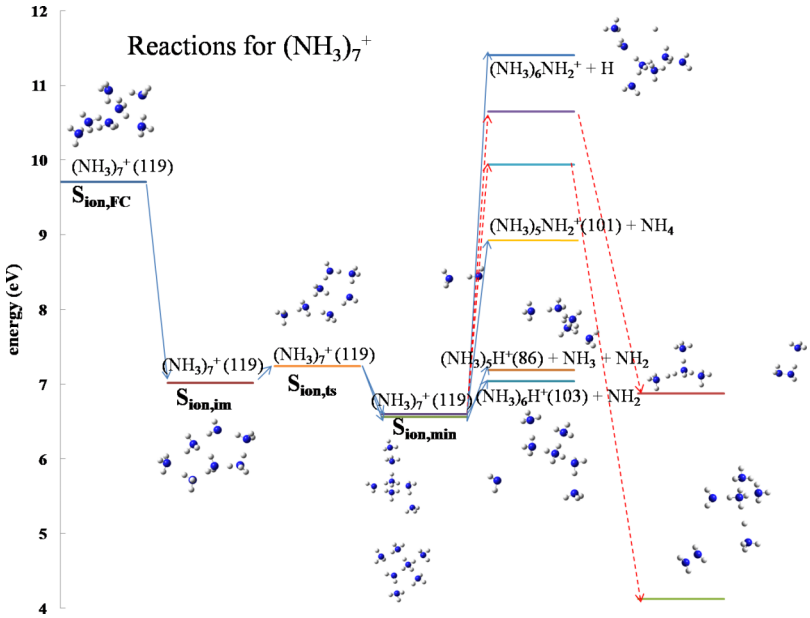

FIG. 13. The detailed dissociation potential surface for $(NH_3)_7^+$. Mass signals $(NH_3)_6H^+$ (103), $(NH_3)_5NH_2^+$ (101), and $(NH_3)_5H^+$ (86) observed in the experiment can be formed within the energy limit based on the calculations. For atoms in the structure, blue is nitrogen and grey is hydrogen. The calculation level is MP2/6-311++G(d,p).

TABLE III. Energy barriers for $(NH_3)_n^+$ (n = 2-7) fragmentation reactions producing $(NH_3)_{n-1}H^+$, $(NH_3)_{n-1}NH_2^+$, $(NH_3)_{n-2}H^+$ ions. The calculation level is MP2/6-311++G(d,p).

	Energy limit ΔE (eV)	$(NH_3)_{n-1}H^+$ Eq. (1) (eV)	$(NH_3)_{n-1}NH_2^+$ Eq. (2) (eV)	$(NH_3)_{n-2}H^+$ Eq. (3) (eV)
$(NH_3)_2^+$	1.86	1.05	...	...
$(NH_3)_3^+$	2.12	0.70	1.72	1.91
$(NH_3)_4^+$	2.12	0.58	2.26	1.47
$(NH_3)_5^+$	2.37	0.49	2.62	1.11
$(NH_3)_6^+$	2.98	0.44	2.62	0.86
$(NH_3)_7^+$	3.15	0.59	2.33	0.63

atom transferred structure with a $NH_4^+\cdots NH_2$ core. After single (10.51 eV) photon absorption, $(NH_3)_n$ are ionized with a VIE ~9.20–10.57 eV; they evolve to the transferred structure $S_{ion,min}$ after passing over a small energy barrier. The energy stored in the $(NH_3)_n^+$ systems for fragmentation reactions increases from 0.69 eV (n = 1) to 3.15 eV (n = 7) as the cluster size increases. Reaction (1) is the main dissociation reaction for nascent $(NH_3)_n^+$, producing $(NH_3)_{n-1}H^+$ (n = 1 to 7, m/z = 18, 35, 52, 69, 86, and 103): these features are observed at both 25 and 95 °C, and they are the most intense mass signals in the mass spectra. Reaction (2), releasing NH_4 instead of an H atom, has reaction barriers close to the energy limit, and thus, product ions $(NH_3)_{n-2}NH_2^+$ (n = 3 and 6, m/z = 33 and 67) are only observed at 95 °C. Generation of $(NH_3)_{n-1}H_2^+$ features for n < 7 has a very high energy barrier; although the energy barrier decreases as the cluster size increases, this reaction is still not expected. The most likely assignments for such features at m/z = 36, 53, 70, 87, and 104 are $(NH_3)_{n-1}(H_2O)H^+$ clusters.

B. Structures, ionization, and available decomposition pathways for ammonia borane cluster ions $(NH_3BH_3)_n^+$

1. Structures and charge distributions for ammonia borane neutral clusters $(NH_3BH_3)_n$ and their cations $(NH_3BH_3)_n^+$

Structures of isolated and solid state ammonia borane have been studied previously,[2,5,8–24,28,29] and based on these results, we calculate structures of neutral clusters $(NH_3BH_3)_n$ (n = 1-3) at the MP2/6-311++G(d,p) level, as shown in Figure 14. The optimized Cartesian x, y, z coordinates of $(NH_3BH_3)_n$ (n = 1-3) are summarized in the supplementary material, Table S3.[57] NH_3BH_3 monomer is a simple molecule with NH_3 and BH_3 groups connected by a N–B bond. NH_3BH_3, at this level, has ∠HNH angles of the NH_3 group all 107.7° and ∠HBH angles of the BH_3 group all 113.8°, displaying tetrahedral form. B–H bond lengths are 1.209 Å, N–H bonds are 1.017 Å, and the B–N bond length connecting these two groups is 1.656 Å. Structure parameters for NH_3BH_3 calculated at the MP2/6-311++G(d,p), CASSCF(12,8)/6-311++G(d,p), and CASSCF(14,14)/6-311++G(d,p) levels, as well as previous calculation at the CCSD(T)/aVTZ level,[10] and the experimental results based on microwave spectroscopy[12] are listed and compared in Table IV. The MP2 result is extremely close to the structure at the CCSD(T) level with bond length differences <0.003 Å and the angle differences <0.1°. Parameter differences between CASSCF and CCSD(T) methods become larger: the biggest difference is the length of B–N bond, which is about 0.052-0.057 Å longer by either CASSCF method. Since the MP2 and CCSD(T) methods are closer to the experimental result, the MP2 result is used in further structure discussions. CASSCF(12,8) and CASSCF(14,14) show similar structure parameters, and the increase of active orbitals does not provide significant improvement for structure predictions.

The structure of neutral $(NH_3BH_3)_2$ consists of two nearly parallel molecules with a dihedral angle ∠B–N–N–B of just 0.037° (Figure 14). Previous studies of the $(NH_3BH_3)_2$ show that the two NH_3BH_3 molecules of the dimer are linked by $N–H^{\delta+}\cdots H^{\delta-}–B$ dihydrogen bonds with an H···H distance in the range 1.7-2.2 Å.[13–20,23,26] In the present study, four dihydrogen bonds are found in the dimer system with an H···H distance ~2.010–2.015 Å. From experimental studies of the dihydrogen bond, ∠N–H···H bonding tends to be more linear than bent (proposed range 117°-171°), and the ∠B–H···H angle tends to be more bent than linear (proposed range 90°-171°).[17] Calculations at the MP2/6-311++G(d,p) level predict ∠N–H···H angles ~144.7°–145.0° and ∠B–H···H angles ~89.4°–89.6°. These results are consistent with those of previous calculations.[13,14,17,19,20] Compared to the monomer,

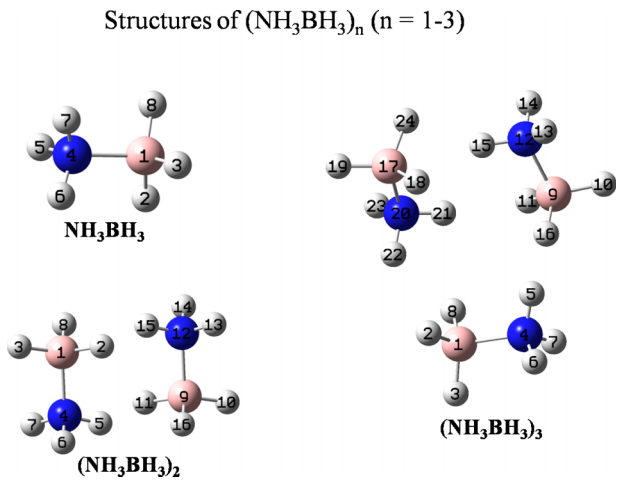

FIG. 14. Optimized structures of neutral $(NH_3BH_3)_n$ (n = 1-3) generated at the MP2/6-311++G(d,p) level. $(NH_3BH_3)_n$ (n = 2-3) form dihydrogen bonds $(N–H^{\delta+}\cdots H^{\delta-}–B)$. For atoms in the structure, blue is nitrogen, pink is boron, and grey is hydrogen.

TABLE IV. Structure parameters for our NH_3BH_3 calculations at the MP2/6-311++G(d,p), CASSCF(12,8)/6-311++G(d,p), and CASSCF(14,14)/6-311++G(d,p) levels, as well as previous calculation at the CCSD(T)/aVTZ level, and the experimental results based on microwave spectroscopy.

	MP2	CASSCF(12,8)	CASSCF(14,14) MOLPRO	CCSD(T)/aVTZ[a]	Expt.[b]
B–H	1.2088	1.2095	1.2090	1.2109	1.2160 ± 0.0017
	1.2088	1.2095	1.2090	1.2109	
	1.2088	1.2098	1.2331	1.2109	
N–H	1.0169	1.0228	1.0232	1.0157	1.0140 ± 0.0020
	1.0170	1.0021	1.0232	1.0157	
	1.0170	1.0021	1.0233	1.0157	
B–N	1.6565	1.7099	1.7143	1.6574	1.6576 ± 0.0016
∠HNH	107.73	107.99	107.74		108.65 ± 0.14
	107.73	107.99	107.74		
	107.73	109.06	107.73		
∠HBH	113.78	114.22	114.20		113.80 ± 0.11
	113.79	114.18	114.16		
	113.79	114.18	114.18		
∠NBH	104.70	104.30	103.91	104.75	104.69 ± 0.11
	104.70	104.30	104.08	104.75	
	104.72	103.99	104.13	104.75	
∠BNH	111.15	109.89	111.10	110.10	110.28 ± 0.14
	111.17	110.90	111.11	110.10	
	111.17	110.90	111.24	110.10	

[a]Reference 10.
[b]Reference 12.

TABLE V. Structure parameters for $(NH_3BH_3)_2$ calculations at the MP2/6-311++G(d,p), CASSCF(12,8)/6-311++G(d,p), and CASSCF(14,14)/6-311++G(d,p) levels, as well as those from previous calculations at MP2/aVTZ and B3LYP/6-311++G(d,p) levels.

	MP2	CASSCF(12,8)	CASSCF(14,14)	MP2/aVTZ[a]	B3LYP/6-311++g(d,p)[b]
B–H	1.214	1.215	1.215	1.214	1.214
	1.215	1.215	1.215	1.214	1.214
	1.206	1.208	1.208	1.204	1.205
	1.215	1.215	1.214	1.214	1.211
	1.215	1.215	1.214	1.214	1.217
	1.206	1.208	1.207	1.204	1.205
N–H	1.017	1.003	1.022	1.014	1.017
	1.017	1.003	1.022	1.014	1.017
	1.025	1.024	1.025	1.023	1.027
	1.017	1.003	1.003	1.014	1.017
	1.017	1.003	1.003	1.014	1.017
	1.025	1.024	1.024	1.023	1.025
B–N	1.632	1.654	1.687/1.655	1.628	1.640
H···H	2.011	2.243	2.241	1.986	1.898
	2.014	2.240	2.245	1.986	2.238
	2.010	2.244	2.235		2.216
	2.015	2.240	2.234		1.965
∠HNB	111.1	111.2	111.2	111.2	111.1
	111.1	111.2	111.2	111.2	111.3
	111.3	111.3	111.4	111.2	111.3
	111.1	111.2	111.4	111.2	111.0
	111.1	111.2	111.5	111.2	111.2
	111.3	111.3	111.6	111.2	111.4
∠HBN	107.2	106.2	105.9		107.3
	105.6	105.5	104.8		105.8
	105.6	105.5	104.8		105.8
	107.2	106.2	106.1		107.3
	105.6	105.5	105.4		106.0
	105.6	105.5	105.4		105.7

[a]Reference 21.
[b]Reference 20.

the B–N bond decreases by 0.024 Å and all B–H and N–H bonds involved in dihydrogen bonds elongate (B–H bonds more than the N–H bonds). Again, these results are consistent with those from previous $(NH_3BH_3)_2$ studies at B3LYP/6-311++G(d,p) level.[20] Structure parameters for $(NH_3BH_3)_2$ calculations at the MP2/6-311++G(d,p), CASSCF(12,8)/6-311++G(d,p), and CASSCF(14,14)/6-311++G(d,p) levels, as well as those from previous calculations at MP2/aVTZ[21] and B3LYP/6-311++G(d,p)[20] levels, are listed and compared in Table V. All the theoretical results are close to each other except for the H···H distances in the dihydrogen bonds N–H···H–B: the two MP2 methods provide similar H···H distances (~1.986–2.015 Å); the B3LYP method yields H···H distances that vary from 1.898 to 2.238 Å; and the H···H distances based on the CASSCF method are ~2.234–2.245 Å. Since all these values fall within the 1.7-2.2 Å experimental range,[2,17,28] one concludes that all the theoretical results are chemically reasonable and acceptable. If the CASSCF active space is expanded from (12,8) to (14,14), the ensuing monomer structure does not evidence any significant difference.

For neutral $(NH_3BH_3)_3$ (Figure 14), two NH_3BH_3 molecules form a parallel structure, as found in the dimer, with the third NH_3BH_3 lying over them. Similar to neutral $(NH_3BH_3)_2$, dihydrogen bonds N–$H^{\delta+}$···$H^{\delta-}$–B are formed in $(NH_3BH_3)_3$ and the H···H distances are in the range 1.805-2.126 Å. The shortest H···H bond is about 0.205 Å smaller than that found for the dimer. The lengths of B–N bonds in $(NH_3BH_3)_3$ are 1.618, 1.621, and 1.634 Å, shorter than the B–N bonds found in the dimer (1.632 Å) and monomer (1.656 Å), consistent with previous findings that the general trend for the B–N bond length is that it becomes shorter in larger systems.[15,18,23,24] Homo-polar B–$H^{\delta-}$···$H^{\delta-}$–B interactions, observed for the NH_3BH_3 crystal,[8] are not found for the neutral $(NH_3BH_3)_3$ cluster.

Structures of $(NH_3BH_3)_n^+$ (n = 1-3) cluster cations in the gas phase differ significantly from those of their respective neutral $(NH_3BH_3)_n$ clusters. Figure 15 shows optimized (adiabatic) structures of $(NH_3BH_3)_n^+$ (n = 1-3) using the MP2/6-311++G(d,p) method and the optimized Cartesian x, y, z coordinates of $(NH_3BH_3)_n^+$ (n = 1-3) are summarized in the supplementary material, Table S3.[57]

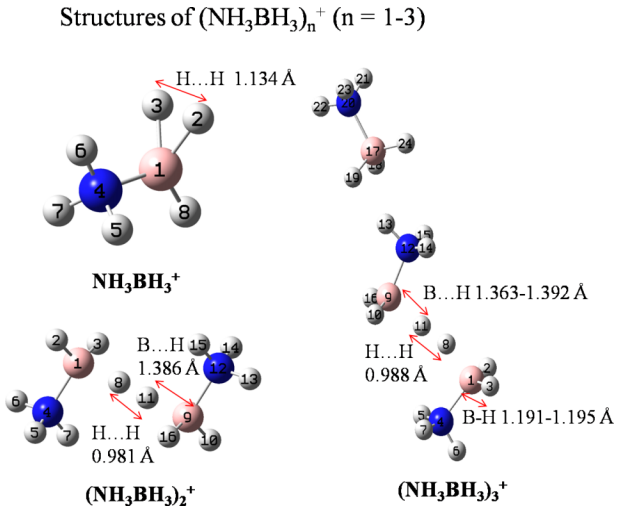

FIG. 15. Optimized structures of $(NH_3BH_3)_n^+$ cations (n = 1-3) generated at the MP2/6-311++G(d,p) level. Two hydrogen atoms of the BH_3 group of $NH_3BH_3^+$ are separated by 1.134 Å. A $B^{\delta+}\cdots H^{\delta-}\cdots{}^{\delta-}H\cdots{}^{\delta+}B$ moiety is formed in $(NH_3BH_3)_2^+$ and $(NH_3BH_3)_3^+$.

The ∠HNH angles of the NH_3 group of $NH_3BH_3^+$ are 105.9°–107°: this gives the NH_3 group a slightly distorted tetrahedral form. On the other hand, in the BH_3 group, ∠HBH angles are 53.1°, 120.0°, and 120.0° and the distance between the two H atoms with the smallest ∠HBH angle is only 1.134 Å. The N–H bond lengths (1.023–1.026 Å) in $NH_3BH_3^+$ are about 0.006–0.009 Å longer than in NH_3BH_3, but the two B–H bond lengths (1.268 Å) forming the ∠HBH angle of 53.1° in the BH_3 group of the cation are about 0.059 Å longer than in the neutral molecule. These results suggest that the B–H bonds are weakened to a greater extent

TABLE VI. $NH_3BH_3^+$ structure parameters obtained from calculation methods (MP2, CASSCF(11,8), CASSCF(13,14)) in basis set 6-311++G(d,p) and from previous results based on the CCSD(T)/aVTZ method.

	MP2/6-311++G(d,p)	CASSCF(11,8)	CASSCF(13,14) MOLPRO	CCSD(T)/aVTZ[a]
B–H	1.2684	1.2672	1.2669	1.2406
	1.2684	1.2673	1.2847	1.2406
	1.1730	1.1699	1.1692	1.1743
N–H	1.0234	1.0112	1.0303	1.0219
	1.0260	1.0294	1.0328	1.0246
	1.0261	1.0320	1.0329	1.0246
B–N	1.5584	1.5584	1.5839	1.5592
∠NBH	113.4	113.7	113.2	113.3
	113.4	113.8	113.4	113.3
	119.6	118.4	119.1	119.9
∠BNH	115.1	115.0	114.9	114.8
	110.5	110.6	110.6	110.6
	110.5	111.4	110.8	110.6
$\theta_{H\text{-}B\text{-}N\text{-}H}$	180.0	179.4	179.8	180.0
	29.1, −29.1	29.4, −30.8	29.5, −29.6	29.1, −29.1
	58.4, −58.5	59.4, −58.3	58.3, −58.8	58.5, −58.5

[a]Reference 9.

than are the N–H bonds. In Table VI, $NH_3BH_3^+$ structure parameters obtained from the present calculation methods (MP2, CASSCF(11,8), CASSCF(13,14)/6-311++G(d,p)) are compared with previous results based on the CCSD(T)/aVTZ method.[9] All three current methods give similar results, with the bond length differences <0.002 Å and angle differences <0.3°; however, the length of the two longest B–H bonds differ for the two sets of calculations (MP2 and CASSCF vs. CCSD(T)) by ~0.028 Å. The B–H bond lengths at the CASSCF level are close to those at the MP2 level with a 0.001 Å difference. Parameters for the CASSCF and CCSD(T) methods diverge somewhat: the biggest difference between the two methods is the length of the longer B–H bonds, which is about 0.026 Å longer by the CASSCF method than by the CCSD(T) method. CASSCF(11,8) and CASSCF(13,14) show similar structure parameters and the increase of active orbitals does not provide significant improvement for structure simulation. Charge distributions for $NH_3BH_3^+$ and NH_3BH_3 are calculated at the MP2 and CASSCF (6-311++G(d,p)) levels, employing the CHELPG method and are summarized in supplementary material, Table S4.[57] The charge on the N atom of $NH_3BH_3^+$ is −0.293, and the B atom has a small positive charge of 0.120. Charges on the H atoms of the NH_3 group are 0.316, 0.316, and 0.293: they are more positive than those on the BH_3 whose H atoms have charges 0.138, 0.139, and −0.029. Since the B and H atoms are all positively charged in $NH_3BH_3^+$, boron should release an H atom more readily than nitrogen. Structural differences between NH_3BH_3 and $NH_3BH_3^+$ are mainly caused by these different charge distributions. As shown in Table S4 for neutral NH_3BH_3,[57] the B atom has a charge of 0.435, and charges on the H atoms of the BH_3 group are −0.267. In the $NH_3BH_3^+$ cation, two B–H bonds of the BH_3 group of $NH_3BH_3^+$ become $B^{\delta+}$–$H^{\delta+}$, which is different from a $B^{\delta+}$–$H^{\delta-}$ covalent bond in NH_3BH_3. Comparing the charge distributions of NH_3BH_3 and $NH_3BH_3^+$, one concludes that the electron is removed from the B–H degenerate orbital of NH_3BH_3 during ionization, and that the B–H bond is the most active region of $NH_3BH_3^+$ for decomposition generating hydrogen and further chemistry. Loss of an electron upon ionization of NH_3BH_3 generates an H…H bond, which is central to the subsequent decomposition chemistry of $NH_3BH_3^+$.

As shown in Figure 15, $(NH_3BH_3)_2^+$ forms an obvious $B^{\delta+}\cdots H^{\delta-}\ldots{}^{\delta-}H\ldots{}^{\delta+}B$ bonding structure. The B–H bond length in the $B^{\delta+}\cdots H^{\delta-}\ldots{}^{\delta-}H\ldots{}^{\delta+}B$ structure is 1.386 Å and the distance between the two H atoms bridging the B atoms of this form is 0.981 Å, 0.243 Å longer than the H–H bond in the H_2 molecule using the same calculation method. Two H atoms bound to the B atom in $NH_3BH_3^+$ form a 1.134 Å H···H bond, while in $(NH_3BH_3)_2^+$, the H···H bond in the $B^{\delta+}\cdots H^{\delta-}\ldots{}^{\delta-}H\ldots{}^{\delta+}B$ structure is even shorter than that in $NH_3BH_3^+$, consistent with the charge distribution results. The bond length between B and N atoms in the dimer cation is 1.598 Å, about 0.040 Å longer than that in $NH_3BH_3^+$. N–H bond lengths are 1.021–1.023 Å, which is almost the same (0.003-0.006 Å shorter) as in the monomer cation. The charge on both B atoms in $(NH_3BH_3)_2^+$ is 0.331, and the charge on the H atoms in the $B^{\delta+}\cdots H^{\delta-}\ldots{}^{\delta-}H\ldots{}^{\delta+}B$ bonding structure is −0.037. Compared to $NH_3BH_3^+$, the B atoms in $(NH_3BH_3)_2^+$ are 0.211 more positive. The H atoms bonded to the B atoms of the dimer are all negatively charged: this charge structure renders the $B^{\delta+}$–$^{\delta-}H$ bond of the cation a more stable charge transfer bond than that of the neutral dimer. Charge distributions for $(NH_3BH_3)_2^+$ and $(NH_3BH_3)_2$ are calculated at the MP2/6-311++G(d,p) level, employing the CHELPG method and are summarized in supplementary material, Table S5.[57] The differences in charge distributions between $NH_3BH_3^+$ and $(NH_3BH_3)_2^+$ are caused by formation of the $B^{\delta+}\cdots H^{\delta-}\ldots{}^{\delta-}H\ldots{}^{\delta+}B$ structure between two NH_3BH_3 units. The homo-polar bridging moiety $B–H^{\delta-}\cdots H^{\delta-}–B$ observed in solid NH_3BH_3 previously[8] is quite different from the $B^{\delta+}\cdots H^{\delta-}\ldots{}^{\delta-}H\ldots{}^{\delta+}B$ moiety found for the $(NH_3BH_3)_2^+$ cation. The distance between two H atoms in the homo-polar structure of the crystal is around 2.03 Å,[8,29] while in $(NH_3BH_3)_2^+$ cation, it is 0.981 Å. Moreover, the B–H bond length in the $B^{\delta+}\cdots H^{\delta-}\ldots{}^{\delta-}H\ldots{}^{\delta+}B$ structure of $(NH_3BH_3)_2^+$ is 1.386 Å, about 0.195 Å longer than the other B–H bond in the dimer cation.

Comparing the charge distributions of $(NH_3BH_3)_2$ and $(NH_3BH_3)_2^+$ as shown in Figure S5,[57] we note that the charge on the N atom in dihydrogen bond N–H···H–B of neutral $(NH_3BH_3)_2$ becomes more negative in the dimer cation (from −0.248 and −0.250 in neutral to −0.410 and −0.411 in cation), while the charges on the H atoms in the N–H···H–B dihydrogen bond for the neutral dimer become more positive in the $(NH_3BH_3)_2^+$ cation. Charges on H atoms connected to N vary from 0.189 (neutral) to 0.297 (cation), and charges on H atoms connect to B vary from −0.245 (neutral) to −0.037 forming a new dihydrogen bond type B–H···H–B. The charges on the B atoms do not change significantly (<0.030) upon cluster ionization. From these calculation results, one can conclude that the electron is removed from the N–H···H–B bond in the neutral clusters, forming a new dihydrogen bond B–H···H–B in the dimer cation. The dihydrogen bond B–H···H–B in $(NH_3BH_3)_2^+$ is the most active region in the cluster ion for hydrogen decomposition reactions: the situation is similar for the trimer ion $(NH_3BH_3)_3^+$.

As shown in Figure 15, the $(NH_3BH_3)_3^+$ trimer cation forms a $B^{\delta+}\cdots H^{\delta-}\ldots{}^{\delta-}H\ldots{}^{\delta+}B$ structure similar to that in the dimer cation. The B···H bond length in the $B^{\delta+}\cdots H^{\delta-}\ldots{}^{\delta-}H\ldots{}^{\delta+}B$ structure is 1.363–1.392 Å, and the distance between the two H atoms at the center of this structure is 0.988 Å. The B–H bond lengths for B atoms in the $B^{\delta+}\cdots H^{\delta-}\ldots{}^{\delta-}H\ldots{}^{\delta+}B$ structure with the other four hydrogen atoms in these BH_3 groups are 1.191–1.195 Å, about 0.168–0.201 Å shorter than the B···H distance in $B^{\delta+}\cdots H^{\delta-}\ldots{}^{\delta-}H\ldots{}^{\delta+}B$ (see the labeling in Figure 15). All these bond lengths around the $B^{\delta+}\cdots H^{\delta-}\ldots{}^{\delta-}H\ldots{}^{\delta+}B$ structure are similar to those found for the dimer cation $(NH_3BH_3)_2^+$ (difference within 0.030 Å). The third B atom in $(NH_3BH_3)_3^+$ forms a dihydrogen bond $N–H^{\delta+}\cdots H^{\delta-}–B$ with the NH_3 group from the nearby NH_3BH_3 molecule as found for the NH_3BH_3 crystal and neutral $(NH_3BH_3)_n$ (n = 2, 3) clusters.[13–20,23,26] The distance between the two H atoms in the $N–H^{\delta+}\cdots H^{\delta-}–B$ dihydrogen bond of $(NH_3BH_3)_3^+$ is 1.798 Å, about the same as calculated for neutral $(NH_3BH_3)_3$. Lengths of the three B–N bonds in $(NH_3BH_3)_3^+$ are in the

range 1.578–1.620 Å, which are about the same as those of the $NH_3BH_3^+$ and $(NH_3BH_3)_2^+$ cations. B atoms in $(NH_3BH_3)_3^+$ are positively charged (0.304, 0.307, and 0.347): the last two values belong to B atoms forming the $B^{\delta+}\cdots H^{\delta-}\cdots{}^{\delta-}H\cdots{}^{\delta+}B$ structure. Charges on the H atoms in $B^{\delta+}\cdots H^{\delta-}\cdots{}^{\delta-}H\cdots{}^{\delta+}B$ moiety are −0.032 and −0.060, close to those found for the dimer cation. Charge distributions for $(NH_3BH_3)_3^+$ and $(NH_3BH_3)_3$ are calculated at the MP2/6-311++G(d,p) level, employing the CHELPG method, and are summarized in supplementary material, Table S6.[57]

In summary, structures of $(NH_3BH_3)_n^+$ (n = 1-3) cations have apparent differences compared to $(NH_3BH_3)_n$ neutral clusters. In $NH_3BH_3^+$, two hydrogen atoms bonded to B are only 1.134 Å apart. In $(NH_3BH_3)_2^+$ and $(NH_3BH_3)_3^+$ cations, a $B^{\delta+}\cdots H^{\delta-}\cdots{}^{\delta-}H\cdots{}^{\delta+}B$ structure is formed and the distance between the two bridging H atoms is 0.981 Å, which is shorter than the H···H bond in $NH_3BH_3^+$. The B···H bond length in the $B^{\delta+}\cdots H^{\delta-}\cdots{}^{\delta-}H\cdots{}^{\delta+}B$ moiety is 1.386 Å, about 0.195 Å longer than a usual B–H bond. The dihydrogen bond $N–H^{\delta+}\cdots H^{\delta-}–B$, observed in the NH_3BH_3 crystal, is identified theoretically in the $(NH_3BH_3)_3^+$ cluster cation, as well as for the neutral clusters $(NH_3BH_3)_2$ and $(NH_3BH_3)_3$.

2. Ammonia borane cluster cation $(NH_3BH_3)_n^+$ (n = 1-3) spin densities and orbitals

Figure 16 shows the spin densities for $(NH_3BH_3)_n^+$ (n = 1-3) calculated at the MP2/6-311++G(d,p) level. The unpaired electron of $NH_3BH_3^+$ is centered around the B atom and the two H atoms bound to it with a short distance (1.134 Å) between them. In the $(NH_3BH_3)_2^+$ cluster ion, the unpaired electron is centered around the $B^{\delta+}\cdots H^{\delta-}\cdots{}^{\delta-}H\cdots{}^{\delta+}B$ structure. The spin density distribution for the $(NH_3BH_3)_3^+$ cluster cation is similar. Spin density value for each atom of $(NH_3BH_3)_n^+$ (n = 1-3), calculated at the MP2/6-311++G(d,p) level for $(NH_3BH_3)_n^+$, is summarized in the supplementary material, Table S7.[57] Based on these calculations, the unpaired electron is most likely to localize on the B atom (n = 1) or the $B^{\delta+}\cdots H^{\delta-}\cdots{}^{\delta-}H\cdots{}^{\delta+}B$ moiety (n = 2, 3). Therefore, these are the most active sites for initiation of dissociation reactions.

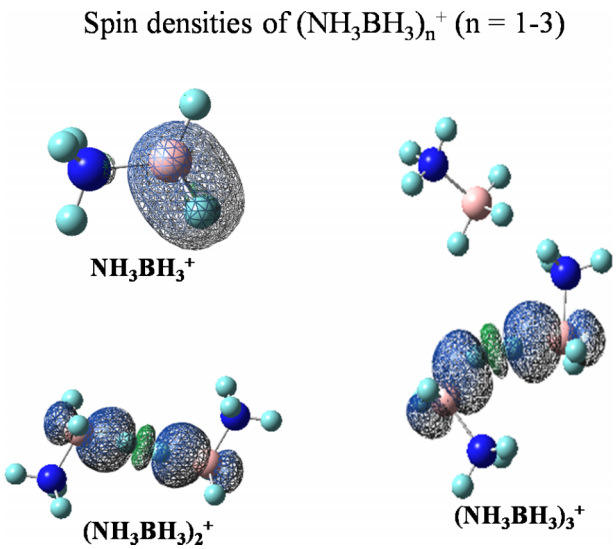

FIG. 16. Spin densities of $(NH_3BH_3)_3^+$ (n = 1-3) cluster cations calculated at the MP2/6-311++G(d,p) level. The unpaired electron is located on the BH_3 group (n = 1) or the $B^{\delta+}\cdots H^{\delta-}\cdots{}^{\delta-}H\cdots{}^{\delta+}B$ moiety (n = 2-3). For atoms in the structure, blue is nitrogen, pink is boron, and green is hydrogen.

Molecular orbitals and NBOs of $(NH_3BH_3)_n^+$ (n = 1-3), calculated at the MP2 and CASSCF(11,8) levels, are provided in the supplementary material, Figures S5–S16.[57] Details of these orbitals are discussed in the supplementary material as well.[57] CASSCF natural bond orbitals apparently provide a more useful bonding description than those generated by the MP2 method, as the CASSCF NBOs provide both σ bonding and antibonding orbital information for the $B^{\delta+}\cdots H^{\delta-}\cdots{}^{\delta-}H\cdots{}^{\delta+}B$ moiety of the $(NH_3BH_3)_n^+$ (n = 2, 3) cluster cations.

3. Ionization and decomposition mechanisms of $(NH_3BH_3)_n^+$ (n = 1-3)

The ionization mechanisms of $(NH_3BH_3)_n$ (n = 1-3) clusters are similar to those calculated for ammonia clusters $(NH_3)_n$: following $(NH_3BH_3)_n$ ionization, these cluster ions evolve to a more stable structure $S_{ion,min}$ after passing through a small energy barrier for cluster cation size n = 2, 3. The NH_3BH_3 monomer, however, forms a stable structure $S_{ion,min}$ without a transition state $S_{ion,ts}$ and an intermediate state $S_{ion,im}$, as presented in Figure 17. The energy difference ΔE is the energy stored in vibrations of the cation system, which can be used for dissociation reactions (Figures 17–19). For n = 2 or 3, the most stable cation structure $S_{ion,min}$ of $(NH_3BH_3)_n^+$ has the $B^{\delta+}\cdots H^{\delta-}\cdots{}^{\delta-}H\cdots{}^{\delta+}B$ moiety. The VIE, AIE, and ΔE values for $(NH_3BH_3)_n$ clusters from our MP2/6-311++G(d,p) calculations, along with those from previous CCSD/aVTZ[9] calculations, and experimental values[11] for the AIE of NH_3BH_3, are summarized in Table VII: the MP2 results underestimate the AIE by 0.40 eV, which is acceptable for the present work. The $B^{\delta+}\cdots H^{\delta-}\cdots{}^{\delta-}H\cdots{}^{\delta+}B$ rearrangement can lower the energy of the particular cation system by almost 1 eV. For all three $(NH_3BH_3)_n$ (n = 1-3) species, the VIE is higher than the 118 nm photon energy (10.51 eV) by 0.02 eV to 0.15 eV; however, as clusters are also heated in the nozzle to 95 °C, these small energy differences, assuming they are real, do not preclude ionization. As $(NH_3BH_3)_n$ clusters are ionized and evolve to local minimum ion structures $S_{ion,min}$, a number of dissociation reactions can occur. For $NH_3BH_3^+$ (Figure 17), a single H atom is released from the BH_3 group: the energy barrier for this process is 0.67 eV, which is within the monomer energy limit (ΔE = 1.54 eV). This fragmentation is the primary dissociation reaction for the $NH_3BH_3^+$ cation. The release of an H atom from the NH_3 group has an energy barrier of 2.66 eV, 1.99 eV higher than the barrier for the BH_3 group. The two H atoms bonded to the B atom with a small ∠HBH of 53.1° can be released from the BH_3 group together, forming an H_2 molecule with energy barrier of 1.08 eV, which is still within the energy limit ΔE for the monomer. From the experimental mass spectra, the ion signal at m/z = 29 is observed and is determined to be mainly $NH_3{}^{10}BH_2^+$ with possible minor contributions from $NH_2{}^{11}BH_2^+$, $NH_3{}^{11}BH^+$, or $NH{}^{11}BH_3^+$. Our calculations show that the H_2 loss channel from $NH_3{}^{11}BH_3^+$ has a substantially greater energy than the H

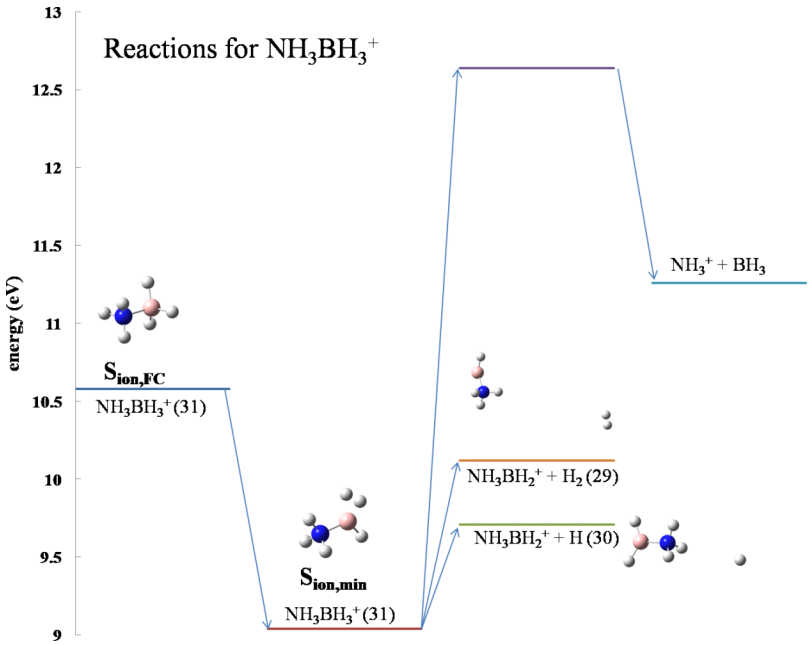

FIG. 17. Possible mechanisms for $NH_3BH_3^+$ fragmentation that generate product ions observed in the experiment. $NH_3BH_3^+$ releasing single H atom has the lowest energy barrier in this system. For atoms in the structure, blue is nitrogen, pink is boron, and grey is hydrogen. The calculation level is MP2/6-311++G(d,p).

loss channel, implying that the reaction, if it occurs, would be negligible. In addition, consideration of the B isotopic ratio confirms that the $m/z = 29$ ion is $NH_3{}^{10}BH_2^+$.

To form a H_2 molecule from neutral NH_3BH_3 on a reasonable, minimally energetic path, one H atom transfers from N to B through an energy barrier of 1.60 eV, and a H_2 molecule can be released from the BH_4 group.[21,22,27] A similar mechanism is explored for $NH_3BH_3^+$; however, the energy barrier is greater than 2.78 eV in the latter case. Moreover, the barrier for B–N bond breaking in NH_3BH_3 is 1.13 eV, whereas it is 3.60 eV for $NH_3BH_3^+$, which is 2.06 eV higher than the energy limit for the cation. Thus, the NH_3^+ signal observed in the experimental mass spectra is not created simply from $NH_3BH_3^+$, but from fragmentation products of $(NH_3BH_3)_n^+$ (n = 2, 3) cations.

Possible reaction mechanisms to explain the mass signals observed for the $(NH_3BH_3)_2^+$ cation are outlined in Figure 18. Starting from the most stable structure of the ion $S_{ion,min}$, as the distance between the two B atoms decreases from the initial 3.752 Å of the neutral ground state to 2.252 Å, one H atom is released from the $B^{\delta+}\cdots H^{\delta-}\cdots{}^{\delta-}H\cdots{}^{\delta+}B$ moiety, forming a $H_3NH_2B\cdots H\cdots BH_2NH_3^+$ rearrangement through an energy barrier of 0.57 eV. Following formation of the single H bridged structure, one of the B–N bonds in the $H_3NH_2B\cdots H\cdots BH_2NH_3^+$ bridge can pass through another transition state $S_{ion,dis,ts}$ (within the energy limit $\Delta E = 2.17$ eV): this species evolves to form an intermediate state $S_{ion,dis,im}$ $BH_3BH_2NH_2\cdots H\cdots NH_3^+$. The $S_{ion,dis,im}$ intermediate state no longer supports an $H_2B\cdots H\cdots BH_2$ structure, but two H bridged bonds are formed between

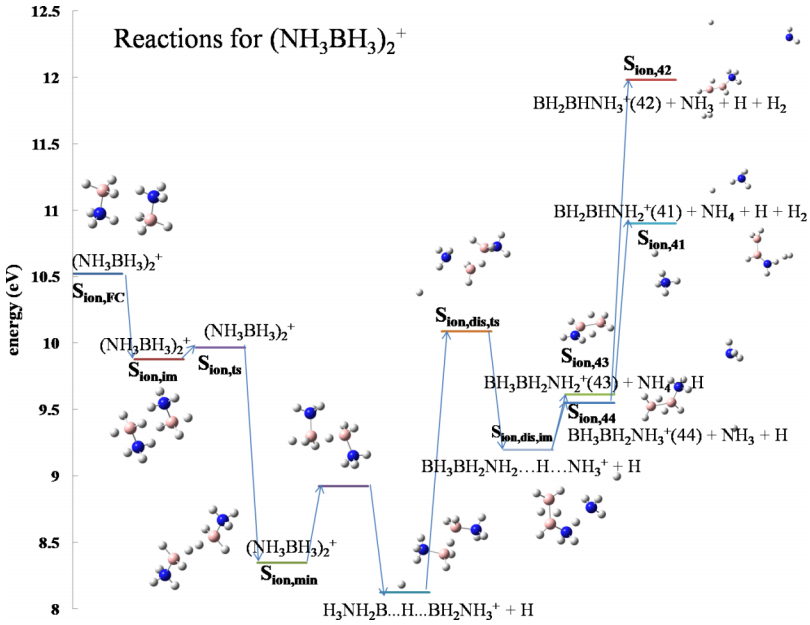

FIG. 18. Possible mechanisms for $(NH_3BH_3)_2^+$ fragmentation that generate product ions observed in the experiment. Dissociation products $S_{ion,44}$ and $S_{ion,43}$ can be formed within the energy limit based on the calculations. For atoms in the structure, blue is nitrogen, pink is boron, and grey is hydrogen. The calculation level is MP2/6-311++G(d,p).

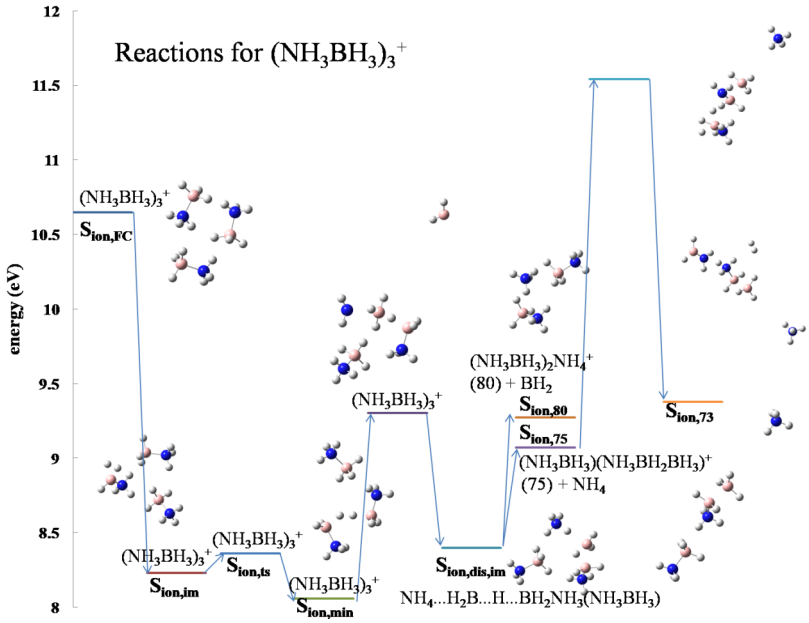

FIG. 19. Possible mechanisms for $(NH_3BH_3)_3^+$ fragmentation that generate product ions observed in the experiment. Dissociation product $S_{ion,80}$ observed can be formed within the energy limit based on the calculations. For atoms in the structure, blue is nitrogen, pink is boron, and grey is hydrogen. The calculation level is MP2/6-311++G(d,p).

BH_2 and BH groups (structure is shown in Figure 18). This intermediate structure stabilizes the molecular system. $S_{ion,dis,im}$ $BH_3BH_2NH_2\cdots H\cdots NH_3^+$ can release either NH_3 or NH_4, forming products $S_{ion,44}$ $BH_3BH_2NH_3$ or $S_{ion,43}$ $BH_3BH_2NH_2$. Each of these two $S_{ion,44}$ and $S_{ion,43}$ products contains two H bridged B···H···B bonds, with a lower barrier for the $S_{ion,44}$ ion. H_2 can be released from the $S_{ion,44}$ and $S_{ion,43}$ products, forming ion products $S_{ion,42}$ and $S_{ion,41}$, respectively. The energy to release H_2 and generate $S_{ion,41}$ from $S_{ion,43}$ is 0.38 eV above the energy limit ΔE, while the energy to release H_2 forming $S_{ion,42}$ from $S_{ion,44}$ is 1.46 eV higher than the limit. Considering the theoretical errors and the energy in the NH_3BH_3 cluster obtained from the heating process, generation of $S_{ion,41}$ from $S_{ion,43}$ might be possible, but generation of $S_{ion,42}$ from $S_{ion,44}$ is unlikely to occur under the present experimental conditions. This result is consistent with the observation that the most intense feature in the mass spectra assigned to the fragmentation of $(NH_3BH_3)_2^+$ is found at $m/z = 44$ as the formation of $S_{ion,43}$ has higher energetic barrier and it can decompose into $S_{ion,41} + H_2$ after the creation. Release of an H atom from $S_{ion,44}$ or $S_{ion,43}$ has an even higher energy barrier. At nozzle temperature ~70 °C, only $m/z = 44$ is observed; as the temperature is increased to 80 °C, mass signals at $m/z = 41$ and 43 are also observed. Mass signal $m/z = 42$ is only observed at nozzle temperature ~95 °C. In previous NH_3BH_3 solid state heating studies, decomposition products at $m/z = 41$ and 42 are reported;[3] therefore, these two observed products may arise from solid NH_3BH_3 (ionized in the interaction region of the TOFMS) rather than from direct ionization of neutral, gas phase $(NH_3BH_3)_2$. Nonetheless, calculations agree with experimental results concerning mass signals at $m/z = 44$ and 43, as a reasonable reaction pathway can be identified within both the $(NH_3BH_3)_2^+$ ion cluster and the energy limit ΔE.

TABLE VII. Vertical ionization energy (VIE), adiabatic ionization energy (AIE), and energy stored (ΔE) in the ion system $(NH_3BH_3)_n^+$, n = 1-3. AIE value of NH_3BH_3 is compared with previous CCSD calculation and experimental work. The calculation level of our work is MP2/6-311++G(d,p).

	VIE	AIE	ΔE	AIE (CCSD)[a]	AIE (Expt.)[b]
NH_3BH_3	10.58	9.04	1.54	9.29	9.44
$(NH_3BH_3)_2$	10.52	8.35	2.17	...	...
$(NH_3BH_3)_3$	10.65	8.06	2.59	...	...

[a]Reference 9.
[b]Reference 11.

For fragmentation reactions of $(NH_3BH_3)_3^+$, a similar set of mechanisms can be generated as discussed above for $(NH_3BH_3)_2^+$, as outlined in Figure 19. The N–B bond in the $B^{\delta+}\cdots H^{\delta-}\cdots{}^{\delta-}H\cdots{}^{\delta+}B$ moiety of $(NH_3BH_3)_3^+$ $S_{ion,min}$ breaks and the distance between two B atoms decreases from its initial 3.535 Å to 2.024 Å forming a stable $NH_4\cdots H_2B\cdots H\cdots BH_2NH_3(NH_3BH_3)^+$ structure $S_{ion,dis,im}$. During this process, an H atom is released from the previous $B^{\delta+}\cdots H^{\delta-}\cdots{}^{\delta-}H\cdots{}^{\delta+}B$ moiety, leading to the formation of a single H bridged entity $H_2B\cdots H\cdots BH_2NH_3$. The released H atom meets with the NH_3 group from the weakened N–B bond to yield a neutral NH_4 group (to the left of the $NH_4\cdots H_2B\cdots H\cdots BH_2NH_3(NH_3BH_3)^+$ $S_{ion,dis,im}$ structure), as shown in Figure 19. This evolution requires surmounting an energy barrier of 1.21 eV, which is within the energy limit. The BH_2 group on the left of the $NH_4\cdots H_2B\cdots H\cdots BH_2NH_3(NH_3BH_3)^+$ $S_{ion,dis,im}$ structure can then dissociate and the ion fragment product $S_{ion,80}$ $NH_4(NH_3BH_3)_2^+$ ($m/z = 80$) can be formed, as observed in the mass spectrum. The NH_4 moiety in the $S_{ion,80}$ ion can form stable dihydrogen bonds N–H···H–B with the nearby BH_3 groups with an H···H distance of 1.586–2.273 Å. The first NH_4 moiety on the left of the $S_{ion,dis,im}$ structure $NH_4\cdots H_2B\cdots H\cdots BH_2NH_3(NH_3BH_3)^+$ can be released as well, and a stable intermediate cation $S_{ion,75}$ $(BH_3BH_2NH_3)(NH_3BH_3)^+$ can be formed with an m/z value of 75. An ion signal with $m/z = 73$ is observed, arising from the ion $S_{ion,75}$ releasing H_2 with a high energy barrier of about 0.89 eV above the energy limit. As the mass signal at $m/z = 73$ is only

observed at 95 °C and the NH_3BH_3 solid starts to decompose at 90 °C, the $m/z = 73$ ion may not originate from the isolated $(NH_3BH_3)_3^+$ cation dissociation reactions, but rather from reactions initiated by the solid compound decomposition at high temperature. The $m/z = 72$ ion observed in the experiment is most likely the B isotope molecule of signal $m/z = 73$ ion.

In summary, based on the spin density calculations for $(NH_3BH_3)_n^+$ (n = 1-3) cationic clusters, the unpaired electron is located around the B atom or more specifically, the $B^{\delta+}\cdots H^{\delta-}\ldots{}^{\delta-}H\ldots{}^{\delta+}B$ moiety if identified: fragmentation reactions are most likely initiated at these two sites. CASSCF derived natural bond orbitals show σ bonding and σ antibonding orbitals around the $B^{\delta+}\cdots H^{\delta-}\ldots{}^{\delta-}H\ldots{}^{\delta+}B$ moiety, which best describes electron occupations and is consistent with the observed and calculated fragmentation reactions. Because the electronic and geometrical structures of the $(NH_3BH_3)_n^+$ cations are significantly different from those of the respective neutral $(NH_3BH_3)_n$ clusters, the neutral and ionic clusters have different dissociation mechanisms. These mechanisms also differ from those found for solid NH_3BH_3. The most energetically favored dissociation reaction for the $NH_3BH_3^+$ monomer is the loss of one H atom, released from the B atom. In $(NH_3BH_3)_n^+$ (n = 2, 3) clusters, the first dissociation step is the breaking of the $B^{\delta+}\cdots H^{\delta-}\ldots{}^{\delta-}H\ldots{}^{\delta+}B$ moiety. The N–B bond then dissociates and the two B atoms in the $B^{\delta+}\cdots H^{\delta-}\ldots{}^{\delta-}H\ldots{}^{\delta+}B$ approach each other, forming a $H_2B\cdots H\cdots BH_2$ arrangement with the release of an H atom.

VI. CONCLUSIONS

Single photon ionization and dissociation mechanisms of ammonia and ammonia borane cluster cations have been investigated through experimental and computational approaches. For ammonia, $(NH_3)_{n-1}H^+$ are the main dissociation products. Other products from $(NH_3)_n^+$ ions (e.g., $(NH_3)_nNH_2^+$ and $(NH_3)_{n-1}(H_2O)H^+$) are observed as well, and their intensity increases as the nozzle temperature is raised from 25 to 95 °C. The only features shared in the mass spectra of $(NH_3BH_3)_n$ and $(NH_3)_n$ are NH_x^+ (x = 0-4): no other common features are observed for m/z above 18. Assignments of $(NH_3BH_3)_n^+$ are rationalized based on the isotopic abundance of B atom. The most intense peak in NH_3BH_3 mass spectra is the $NH_3BH_2^+$ ion. $(NH_3BH_3)_2$ and $(NH_3BH_3)_3$ clusters readily lose H_2.

Initial dissociation mechanisms, potential energy surfaces for ionized NH_3 and NH_3BH_3, and their clusters are calculated at the MP2/6-311++G(d,p) level. The ammonia cluster cations $(NH_3)_n^+$ decomposition reactions can be summarized as

$$(NH_3)_n^+ \rightarrow (NH_3)_{n-1}H^+ + NH_2 \quad (1')$$

$$(NH_3)_n^+ \rightarrow (NH_3)_{n-2}NH_2^+ + NH_4 \quad (2')$$

$$(NH_3)_{n-1}H^+ \rightarrow (NH_3)_{n-2}H^+ + NH_3. \quad (3')$$

Reaction (1′) has the lowest energy barrier, which decreases from 1.05 eV to 0.22 eV as the cluster number n increases. The energy barrier for reaction (2′) is close to the energy limit ΔE in the cation system, while for reaction (3′), similar to reaction (1′), the energy barriers decrease from 1.91 eV to 0.63 eV as the cluster number n increases.

Structures of $(NH_3BH_3)_n^+$ (n = 1-3) cations have significant differences compared to their respective $(NH_3BH_3)_n$ neutral clusters. In $NH_3BH_3^+$, two H atoms connected to the B atom have separation of 1.134 Å. In $(NH_3BH_3)_2^+$ and $(NH_3BH_3)_3^+$ cations, a $B^{\delta+}\cdots H^{\delta-}\ldots{}^{\delta-}H\ldots{}^{\delta+}B$ moiety is formed and the distance between the two bonded H atoms is 0.981–0.988 Å: this structure is not the homopolar $B–H^{\delta-}\cdots H^{\delta-}–B$ structure observed for solid NH_3BH_3. The dihydrogen $N–H^{\delta+}\cdots H^{\delta-}–B$ bond structure characterized in the NH_3BH_3 crystal is also found theoretically for $(NH_3BH_3)_3^+$ cationic clusters and neutral clusters $(NH_3BH_3)_2$ and $(NH_3BH_3)_3$.

The N atom has the most negative charge in NH_3BH_3 system. Based on spin density maps, the unpaired electron (hole) for these ions is localized on the B atom. From the study of molecular orbitals and natural bond orbitals of $(NH_3BH_3)_n^+$ clusters, CASSCF derived natural bond orbitals best represent electron occupations and are consistent with the observed and calculated fragmentation pathway. Because structures of $(NH_3BH_3)_n^+$ cations are significantly different from their respective neutral $(NH_3BH_3)_n$ structures, they have different dissociation mechanisms than does the NH_3BH_3 solid. The lowest energy dissociation reaction for $NH_3BH_3^+$ monomer is loss of one H atom from the B atom. For cluster cations $(NH_3BH_3)_n^+$ (n = 2, 3), the first dissociation step is the breaking of $B^{\delta+}\cdots H^{\delta-}\ldots{}^{\delta-}H\ldots{}^{\delta+}B$ bonding moiety. Following this initial step, the N–B bond breaks and the two B atoms in the $B^{\delta+}\cdots H^{\delta-}\ldots{}^{\delta-}H\ldots{}^{\delta+}B$ moiety move toward one another, forming a $H_2B\cdots H\cdots BH_2$ structure: CASSCF natural bond orbitals represent this behavior more clearly than other orbital presentation plots.

ACKNOWLEDGMENTS

This study is supported by a grant from the U.S. Army Research Office (ARO, Nos. FA9550-10-1-0454 and W911-NF13-10192) and in part by the U.S. National Science Foundation (NSF) through the XSEDE supercomputer resources provided by NCSA under Grant No. TG-CHE110083. We want to thank Professor Atanu Bhattacharya, of the Department of Inorganic and Physical Chemistry, Indian Institute of Science, Bangalore, for his early contributions to this study and his useful discussions concerning NH_3BH_3 decomposition.

[1]A. K. Figen, M. B. Piskin, B. Coskuner, and V. Imamoglu, "Synthesis, structural characterization, and hydrolysis of ammonia borane (NH_3BH_3) as a hydrogen storage carrier," Int. J. Hydrogen Energy **38**, 16215 (2013).
[2]Ch. B. Lingam, K. R. Babu, S. P. Tewari, and G. Vaitheeswaran, "Structure, electronic, bonding, and elastic properties of NH_3BH_3: A density functional study," J. Comput. Chem. **32**, 2298 (2011).
[3]O. Palumbo, A. Paolone, P. Rispoli, R. Cantelli, and T. Autrey, "Decomposition of NH_3BH_3 at sub-ambient pressures: A combined thermogravimetry-differential thermal analysis-mass spectrometry study," J. Power Sources **195**, 1615 (2010).
[4]L. H. Jepsen, V. Ban, K. T. Moller, Y.-S. Lee, Y. W. Cho, F. Besenbacher, Y. Filinchuk, J. Skibsted, and T. R. Jensen, "Synthesis, crystal structure, thermal decomposition, and 11B MAS NMR characterization of $Mg(BH_4)_2(NH_3BH_3)_2$," J. Phys. Chem. **118**, 12141 (2014).

[5]Y. Huang, X. Huang, Z. Zhao, W. Li, S. Liang, D. Duan, K. Bao, Q. Zhou, B. Liu, and T. Cui, "Experimental verification of the high pressure crystal structure in NH_3BH_3," J. Chem. Phys. **140**, 244507 (2014).
[6]R. L. Sams, S. S. Xantheas, and T. A. Blake, "Vapor phase infrared spectroscopy and *ab initio* fundamental anharmonic frequencies of ammonia borane," J. Phys. Chem. A **116**, 3124 (2012).
[7]Y.-S. He, K.-F. Chen, C.-H. Lin, M.-T. Lin, C.-C. Chen, and C.-H. Lin, "Use of an accelerometer and a microphone as gas detectors in the online quantitative detection of hydrogen released from ammonia borane by gas chromatography," Anal. Chem. **85**, 3303 (2013).
[8]Y. Yao, X. Yong, J. S. Tse, and M. J. Greschner, "Dihydrogen bonding in compressed ammonia borane and its roles in structural stability," J. Phys. Chem. C **118**, 29591 (2014).
[9]M. H. Matus, D. J. Grant, M. T. Nguyen, and D. A. Dixon, "Fundamental thermochemical properties of ammonia borane and dehydrogenated derivatives (BNH_n, n = 0–6)," J. Phys. Chem. C **113**, 16553 (2009).
[10]D. A. Dixon and M. Gutowski, "Thermodynamic properties of molecular borane amines and the $[BH_4^-][NH_4^+]$ salt for chemical hydrogen storage systems from *ab initio* electronic structure theory," J. Phys. Chem. A **109**, 5129 (2005).
[11]D. R. Lloyd and N. Lynaugh, "Photoelectron studies of boron compounds. III. Complexes of borane with Lewis bases," J. Chem. Soc., Faraday Trans. **2**(68), 947 (1972).
[12]L. R. Thorne, R. D. Suenram, and F. J. Lovas, "Microwave spectrum, torsional barrier and structure of BH_3NH_3," J. Chem. Phys. **78**(1), 167 (1983).
[13]T. Kar and S. Scheiner, "Comparison between hydrogen and dihydrogen bonds among H_3BNH_3, H_2BNH_2, and NH_3," J. Chem. Phys. **119**, 1473 (2003).
[14]T. B. Richardson, S. de Gala, and R. H. Crabtree, "Unconventional hydrogen bonds: Intermolecular B–H· · ·H–N interactions," J. Am. Chem. Soc. **117**, 12875 (1995).
[15]A. Staubitz, A. P. M. Robertson, and I. Manners, "Ammonia-borane and related compounds as dihydrogen sources," Chem. Rev. **110**, 4079 (2010).
[16]C. A. Morrison and M. M. Siddick, "Dihydrogen bonds in solid BH_3NH_3," Angew. Chem., Int. Ed. **43**, 4780 (2004).
[17]W. T. Klooster, T. F. Koetzle, P. E. M. Siegbahn, T. B. Richardson, and R. H. Crabtree, "Study of the N–H· · ·H–B dihydrogen bond including the crystal structure of BH_3NH_3 by neutron diffraction," J. Am. Chem. Soc. **121**, 6337 (1999).
[18]P. L. Popelier, "Characterization of a dihydrogen bond on the basis of the electron density," J. Phys. Chem. A **102**, 1873 (1998).
[19]R. H. Crabtree, P. E. M. Siegbahn, O. Eisenstein, A. L. Rheingold, and T. F. Koetzle, "A new intermolecular interaction: Unconventional hydrogen bonds with element-hydride bonds as proton acceptor," Acc. Chem. Res. **29**, 348 (1996).
[20]Y. Meng, Z. Zhou, C. Duan, B. Wang, and Q. Zhong, "Non-conventional hydrogen bonding interaction of BH_3NH_3 complexes: A comparative theoretical study," J. Mol. Struct.: THEOCHEM **713**, 135 (2005).
[21]V. S. Nguyen, M. H. Matus, D. J. Grant, M. T. Nguyen, and D. A. Dixon, "Computational study of the release of H_2 from ammonia borane dimer $(NH_3BH_3)_2$ and its ion pair isomers," J. Phys. Chem. A **111**, 8844 (2007).
[22]M. T. Nguyen, V. S. Nguyen, M. H. Matus, G. Gopakumar, and D. A. Dixon, "Molecular mechanism for H_2 release from NH_3BH_3, including the catalytic role of the Lewis acid BH_3," J. Phys. Chem. A **111**, 679 (2007).
[23]M. P. Mitoraj, "Bonding in ammonia borane: An analysis based on the natural orbitals for chemical valence and the extended transition state method (ETS-NOCV)," J. Phys. Chem. A **115**, 14708 (2011).
[24]J. Dillen and P. Verhoeven, "The end of a 30-year-old controversy? A computational study of the B–N stretching frequency of BH_3–NH_3 in the solid state," J. Phys. Chem. A **107**, 2570 (2003).
[25]R. Cantelli, A. Paolone, O. Palumbo, F. Leardini, T. Autrey, A. Karkamkar, and A. T. Luedtke, "Rotational dynamics in ammonia borane: Evidence of strong isotope effects," J. Alloy. Compd. **580**, S63 (2013).
[26]O. Gunaydin-Sen, R. Achey, N. S. Dalal, A. Stowe, and T. Autrey, "High resolution 15N NMR of the 225 K phase transition of ammonia borane (NH_3BH_3): Mixed order-disorder and displaive behavior," J. Phys. Chem. B **111**, 677 (2007).
[27]Y. Liang and J. S. Tse, "First-principles study on the mechanisms for H_2 formation in ammonia borane at ambient and high pressure," J. Phys. Chem. C **116**, 2146 (2012).
[28]S. Trudel and D. F. R. Gilson, "High-pressure Raman spectroscopic study of the ammonia-borane complex. Evidence for the dihydrogen bond," Inorg. Chem. **42**, 2814 (2003).
[29]D. J. Wolstenholme, J. L. Dobson, and G. S. McGrady, "Homopolar dihydrogen bonding in main group hydrides: Discovery, consequences, and applications," Dalton Trans. **44**, 9718 (2015).
[30]Y. Hu and E. R. Bernstein, "Vibrational and photoionization spectroscopy of biomolecules: Aliphatic amino acid structures," J. Chem. Phys. **128**, 164311 (2008).
[31]J. Guan, Y. Hu, H. Zou, L. Cao, F. Liu, X. Shan, and L. Sheng, "Competitive fragmentation pathways of acetic acid dimer explored by synchrontron VUV photoionization mass spectrometry and electronic structure calculations," J. Chem. Phys. **137**, 124308 (2012).
[32]F. Dong, S. Heinbuch, J. J. Rocca, and E. R. Bernstein, "Dynamics and fragmentation of van der Waals clusters: $(H_2O)_n$, $(CH_3OH)_n$, and $(NH_3)_n$ upon ionization by a 26.5 eV soft x-ray laser," J. Chem. Phys. **124**, 224319 (2006).
[33]F. Dong, S. Heinbuch, J. J. Rocca, and E. R. Bernstein, "Single photon ionization of van der Waals clusters with a soft x-ray laser: $(SO_2)_n$ and $(SO_2)_n(H_2O)_m$," J. Chem. Phys. **125**, 154317 (2006).
[34]S. Heinbuch, F. Dong, J. J. Rocca, and E. R. Bernstein, "Single photon ionization of van der Waals clusters with a soft x-ray laser: $(CO_2)_n$ and $(CO_2)_n(H_2O)_m$," J. Chem. Phys. **125**, 154316 (2006).
[35]H. Shinohara and N. Nishi, "Multiphoton ionization mass spectroscopic detection of ammonia clusters," Chem. Phys. Lett. **87**, 561 (1982).
[36]H. Shinohara and N. Nishi, "Photoionization of ammonia clusters: Detection and distribution of unprotonated cluster ions $(NH_3)_n^+$, n = 2-25," J. Chem. Phys. **83**, 1939 (1985).
[37]P. E. Janeiro-Barral and M. Mella, "Study of the structure, energetics and vibrational properties of small ammonia clusters $(NH_3)_n$ (n = 2-5) using correlated *ab initio* methods," J. Phys. Chem. A **110**, 11244 (2006).
[38]F. M. Abu-Awwad, "A comparative study of structure and electrostatic potential of hydrogen-bonded clusters of neutral ammonia $(NH_3)_n$ (n = 2-6)," J. Mol. Struct. **683**, 57 (2004).
[39]L. Yu and Z.-Z. Yang, "Study on structures and properties of ammonia clusters $(NH_3)_n$ (n = 1-5) and liquid ammonia in terms of *ab initio* method and atom-bond electronegativity equalization method ammonia-8P fluctuating charge potential model," J. Chem. Phys. **132**, 174109 (2010).
[40]P. E. Janeiro-Barral, M. Mella, and E. Curotto, "Structure and energetics of ammonia clusters $(NH_3)_n$ (n = 3-20) investigated using a rigid-polarizable model derived from *ab initio* calculations," J. Phys. Chem. A **112**, 2888 (2008).
[41]M. Patrone and M. Mella, "Sequential growth simulation of $(NH_3)_n$ clusters (n = 2-8) in ultracold superfluid environment," Chem. Phys. Lett. **514**, 16 (2011).
[42]S. A. Kulkarni and R. K. Pathak, "*Ab initio* investigations on neutral clusters of ammonia: $(NH_3)_n$ (n = 2-6)," Chem. Phys. Lett. **336**, 278 (2001).
[43]J. C. Greer, R. Ahlrichs, and I. V. Hertel, "Binding energies and structures of NH_3 clusters," Chem. Phys. **133**, 191 (1989).
[44]T. A. Beu and U. Buck, "Structure of ammonia clusters from n = 3 to 18," J. Chem. Phys. **114**, 7848 (2001).
[45]J. K. Park, "*Ab initio* studies for geometrical structures of ammonia cluster cations," J. Phys. Chem. A **104**, 5093 (2000).
[46]Y. Matsuda, N. Mikami, and A. Fujii, "Vibrational spectroscopy of size-selected neutral and cationic clusters combined with vacuum-ultraviolet one-photon ionization detection," Phys. Chem. Chem. Phys. **11**, 1279 (2009).
[47]M. Hachiya, Y. Matsuda, K.-i. Suhara, N. Mikami, and A. Fujii, "Infrared predissociation spectroscopy of clusters of protic molecules $(NH_3)_n^+$, n = 2-4 and $(CH_3OH)_n^+$, n = 2,3," J. Chem. Phys. **129**, 094306 (2008).
[48]S. Tomoda and K. Kimura, "Equilibrium structure and two kinds of dissociation energy of the ammonia dimer cation $H_3NH^+ \cdots NH_2$," Chem. Phys. Lett. **121**, 159 (1985).
[49]H. Shinohara, N. Nishi, and N. Washida, "Photoionization of ammonia clusters in a pulsed supersonic nozzle beam by vacuum-UV rare-gas resonance lines," Chem. Phys. Lett. **106**, 302 (1984).
[50]W. R. Peifer, M. T. Coolbaugh, and J. F. Garvey, "Observation of 'magic numbers' in the population distributions of the $(NH_3)_{n-1}NH_2^+$ and $(NH_3)_nH_2^+$ cluster ions: Implications for cluster ion structures," J. Chem. Phys. **91**, 6684 (1989).
[51]S. A. Buzza, S. Wei, J. Purnell, and A. W. Castleman, "Formation and metastable decomposition of unprotonated ammonia cluster ions upon femtosecond ionization," J. Chem. Phys. **102**, 4832 (1995).
[52]J. Purnell, S. Wei, S. A. Buzza, and A. W. Castleman, Jr., "Formation and protonated ammonia clusters probed by a femtosecond laser," J. Phys. Chem. **97**, 12530 (1993).
[53]Y. Q. Guo, A. Bhattacharya, and E. R. Bernstein, "Decomposition of nitramine energetic materials in excited electronic states: RDX and HMX," J. Chem. Phys. **122**, 244310 (2005).

[54]Y. Q. Guo, M. Greenfield, A. Bhattacharya, and E. R. Bernstein, "On the excited electronic state dissociation of nitramine energetic materials and model systems," J. Chem. Phys. **127**, 154301 (2007).
[55]H.-S. Im and E. R. Bernstein, "On the initial steps in the decomposition of energetic materials from excited electronic states," J. Chem. Phys. **113**, 7911 (2000).
[56]H.-S. Im and E. R. Bernstein, "Photodissociation of NO_2 in the region 217–237 nm: Nascent no energy distribution and mechanism," J. Phys. Chem. A **106**, 7565 (2002).
[57]See supplementary material at http://dx.doi.org/10.1063/1.4945624 for the active spaces of CASSCF calculation for $(NH_3BH_3)_n$ and $(NH_3BH_3)_n^+$ (n = 1-3), orbitals in MP2 and CASSCF methods for $(NH_3BH_3)_n^+$ (n = 1-3), charge distributions and spin densities of $(NH_3BH_3)_n^+$ (n = 1-3), BSSE corrections of $(NH_3)_n^+$ (n = 1-4) reactions, optimized cartesian x, y, z coordinates of $(NH_3)_n$, $(NH_3)_n^+$, $(NH_3BH_3)_n$ and $(NH_3BH_3)_n^+$.
[58]F. C. Pickard IV, M. E. Dunn, and G. C. Shields, "Comparison of model chemistry and density functional theory thermochemical predictions with experiment for formation of ionic clusters of the ammonium cation complexed with water and ammonia; atmospheric implications," J. Phys. Chem. A **109**, 4905 (2005).
[59]I. N. Tang and A. W. Castleman, Jr., "Gas-phase solvation of the ammonium ion in ammonia," J. Chem. Phys. **62**, 4576 (1975).
[60]J. D. Payzant, A. J. Cunningham, and P. Kebarle, "Gas phase solvation of the ammonium ion by NH_3 and H_2O and stabilities of mixed clusters $NH_4^+(NH_3)_n(H_2O)_w$," Can. J. Chem. **51**, 3242 (1973).
[61]A. W. Castleman, Jr., W. B. Tzeng, S. Wei, and S. Morgan, "Photophysics of clusters intracluster reactions and dynamics of dissociation processes," J. Chem. Soc., Faraday. Trans. **86**, 2417 (1990).
[62]S. T. Ceyer, P. W. Tiedemann, B. H. Mahan, and Y. T. Lee, "Energetics of gas phase proton solvation by NH_3," J. Chem. Phys. **70**, 14 (1979).
[63]J. J. Breen, W.-B. Tzeng, K. Kilgore, R. G. Keesee, and A. W. Castleman, Jr., "Intracluster reactions in phenylacetylene ammonia clusters initiated through resonant enhanced ionization," J. Chem. Phys. **90**, 19 (1989).